MLL1 is required for maintenance of intestinal stem cells and the expression of the cell adhesion molecule JAML

Neha Goveas[1], Claudia Waskow[2,#a,#b], Kathrin Arndt[2], Julian Heuberger[3,#c], Qinyu Zhang[1], Dimitra Alexopoulou[4], Andreas Dahl[4], Walter Birchmeier[3], Konstantinos Anastassiadis[5], A. Francis Stewart[1,6*], Andrea Kranz[1*]

[1] Genomics, Center for Molecular and Cellular Bioengineering, Biotechnology Center, Technische Universität Dresden, Dresden, Germany

[2] Institute for Immunology and Department of Medicine III, Technische Universität Dresden, Dresden, Germany

[3] Laboratory of Signal Transduction in Development and Cancer, Max Delbrück Center for Molecular Medicine, Berlin, Germany

[4] DRESDEN-concept Genome Center, Center for Molecular and Cellular Bioengineering, Technische Universität Dresden, Dresden, Germany

[5] Stem Cell Engineering, Center for Molecular and Cellular Bioengineering, Biotechnology Center, Technische Universität Dresden, Dresden, Germany

[6] Max Planck Institute of Molecular Cell Biology and Genetics, Dresden, Germany

[#a]Current Address: Regeneration in Hematopoiesis, Leibniz-Institute on Aging, Fritz-Lipmann-Institute (FLI), Jena, Germany

[#b]Current Address: Institute of Biochemistry and Biophysics, Faculty of Biological Sciences, Friedrich-Schiller-Universität Jena, Jena, Germany

[#c]Current Address: Department of Hepatology and Gastroenterology, Charité University Medicine, Berlin, Germany

* Corresponding authors

E-mail: francis.stewart@tu-dresden.de (AFS)

E-mail: andrea.kranz@tu-dresden.de (AK)

Abstract

Epigenetic control is crucial for lineage-specific gene expression that creates cellular identity during mammalian development and in adult organism. Histone 3 lysine 4 methylation (H3K4) is a universal epigenetic mark. Mixed lineage leukemia (MLL1) is the founding member of the mammalian family of H3K4 methyltransferases. It was originally discovered as the main gene mutated in early onset leukemias and then found to be required for hematopoietic stem cell development and maintenance. However, the roles of MLL1 in non-hematopoietic tissues remain largely unexplored. To bypass hematopoietic lethality, we used bone marrow transplantation and conditional mutagenesis to discover that the most overt phenotype in *Mll1*-mutant mice is intestinal failure. Loss of MLL1 is accompanied by a differentiation bias towards the secretory lineage with increased numbers of goblet cells. MLL1 is expressed in intestinal stem cells (ISCs) and transit amplifying (TA) cells but at reduced levels in Paneth cells and not in the villus. MLL1 is required for the maintenance of intestinal stem cells (ISCs) and proliferation in the crypt. Transcriptome analysis implicate MLL1-dependent expression in ISCs of several transcription factors including *Pitx2, Gata4, Foxa1* and *Onecut2*, and also a cell adhesion molecule, *Jaml*. Reactive transcriptome changes in Paneth cells and organoids imply that JAML plays a key role in the crypt stem cell niche. All known postnatal functions of MLL1 relate to stem cell maintenance and lineage decisions thereby highlighting the suggestion that MLL1 is a master stem cell regulator.

Author Summary

The ability of adult stem cells to produce functional progenies through differentiation is critical to maintain function and integrity of organs. A fundamental challenge is to identify factors that control the transition from self-renewal to the differentiated state. Epigenetic factors amongst others can fullfill such a role. Methylation of histone 3 on lysine 4 (H3K4) is a posttranslational epigenetic modification that is associated with actively transcribed genes. In mammals, this epigenetic mark is catalyzed by one of six H3K4 methyltransferases, including the founding member of the family, MLL1. MLL1 is important for the precise functioning of the hematopoietic stem cell compartment. This raises the possibility of similar functions in other adult stem cell compartments. Due to its intense self-renewal kinetics and its simple repetitive architecture, the intestinal epithelium serves as a prime model for studying adult stem cells. We demonstrate that MLL1 controls intestinal stem cell proliferation and differentiation. Additionally, transcriptome analysis suggests a pertubation in the close interaction between intestinal stem cells and neighbouring Paneth cells through loss of junction adhesion molecule like (JAML). Our work sheds new light on the function of MLL1 for the control of intestinal stem cell identity.

Introduction

Stem cells are cornerstones of tissue biology, ensuring homeostasis and regeneration in many organs, including epithelial tissues such as skin, intestine and mammary gland [1]. Stem cells are characterized by multipotency, which is the ability to differentiate into a restricted number of defined cell types, and self-renewal, which is the capacity to undergo infinite replicative cycles without losing stem cell identity [2]. The remarkable capacities of stem cells, particularly the restricted specificities of multipotency, rely on interplays between specific transcription factors and distinct epigenetic landscapes. Whereas the transcription factors involved in stem cell maintenance and differentiation have been clearly defined, epigenetic contributions are proving more elusive. For example, the transcription factor hierarchies in the stem cell paradigm, hematopoiesis, have been elegantly dissected [3]. However the contributions of DNA and histone methyltransferases to hematopoiesis are still emerging and indicate both specificities and the deeper complexities of epigenetic regulation[4-8].

Methylation of histone 3 on lysine 4 (H3K4) is one of the most conserved and widespread epigenetic systems [9]. H3K4 is methylated in euchromatic regions, with trimethylated H3K4 (H3K4me3) on nucleosomes surrounding active promoters, H3K4me2 marking transcribed regions and H3K4me1 relating to enhancers and active chromatin in general [10-14]. Mammals have six Set1/Trithorax-related methyltransferases that are encoded by three pairs of paralogous sister genes namely, *Mll1* (*Kmt2a*) and *Mll2* (*Kmt2b*), *Mll3* (*Kmt2c*) and *Mll4* (*Kmt2d*), *Setd1a* (*Kmt2f*) and *Setd1b*

102 (*Kmt2g*). Each of the six methyltransferases reside in their own, large, protein
103 complex. However all six complexes are based on a four membered scaffold
104 termed WRAD for the subunits WDR5, RBBP5, ASH2L and DPY30 [15].
105 Functional differences between the six complexes potentially arise from the
106 presence of additional subunits, which are usually shared by paralogous pairs
107 or sometimes uniquely found in one of the six complexes.

108 Mixed lineage leukemia (*MLL1*) was the first mammalian gene
109 identified as a Trithorax homologue and subsequently found to encode a
110 mammalian Set1/Trithorax-type H3K4 methyltransferase (HMT) [16, 17]. In
111 mice, MLL1 is first required at embryonic day 12.5 (E12.5) for definitive
112 hematopoiesis [18, 19] and also required for the maintenance of adult
113 hematopoietic stem cells (HSCs) [20, 21]. *MLL1*, but not its paralogue, *MLL2,*
114 is a proto-oncogene because it can be activated by chromosomal
115 translocations to promote leukemias without additional mutagenesis [22, 23].
116 Over 80 translocation partners have been identified including AF6 and AF9
117 [24]. Notably, *MLL1-AF6* and *-AF9* leukemias rely on *Mll2* expression [6].
118 Mouse studies also indicated that *MLL1-AF9* leukemiogenesis is entirely
119 conveyed by overexpression of *Hoxa9* [25]. Conditional mutagenesis has also
120 revealed MLL1 functions in satellite cells [26] and postnatal neural stem cells
121 (NSCs) [27]. These observations raise the possibility that MLL1 regulates
122 specific functions in stem cell compartments.

123 Due to its high turnover and hierarchical architecture, intestinal stem
124 cells (ISCs) in the intestinal epithelium have become an adult stem cell
125 paradigm. ISCs have been identified as either actively cycling crypt base
126 columnar cells (CBCs) or quiescent label-retaining cells (LRCs) located at the

127 +4 position from the crypt base [28]. Leucine-rich repeat-containing G protein-
128 coupled receptor 5 (LGR5) is one of the best-characterized markers for the
129 CBC class ISCs [29]. They generate transit amplifying (TA) daughter cells that
130 give rise to the terminally differentiated progenies: absorptive enterocytes,
131 secretory goblet, enteroendocrine and Paneth cells [30]. Except for Paneth
132 cells, these cell types take 3 to 5 days to migrate up the villi and are shed into
133 the intestinal lumen. Paneth cells reside at the base of the crypts in close
134 association with ISCs and turn over at a slower rate [30].

135 The quiescent LRCs are active only during stress or injury. They
136 represent a stem cell reserve to replace damaged ISCs [31]. Enterocytes,
137 preterminal enteroendocrine cells, goblet cell precursors and Dll1^{+} secretory
138 progenitors are also notable for their plasticity and can serve as a reservoir for
139 lost stem cells [32, 33] [34]. Mature Paneth cells also show an injury-activated
140 conversion to a stem cell like state [35]. Together with new perceptions in
141 hematopoiesis [4, 6, 36], the dynamic plasticity of the intestinal crypt has
142 expanded the stem cell paradigm [37], especially during replenishment after
143 damage or inflammation.

144 To examine whether MLL1 plays additional roles in the adult, we
145 employed ligand-induced conditional mutagenesis using a tamoxifen-inducible
146 *Rosa26-CreERT2* line (*RC*) for near-ubiquitous Cre recombination to discover
147 that MLL1 is required for the maintenance of the ISC compartment and the
148 balance between secretory and absorptive cell lineages in the adult intestine.

149 ## Results

150

151 **Intestinal functions collapse after loss of MLL1 in adult mice**

152 To explore MLL1 functions, we utilized a multipurpose allele that can
153 be converted from one state to another using FLP and Cre recombination
154 (S1A-S1C Figs) [38, 39]. Homozygous embryos carrying the targeted allele,
155 *Mll1*$^{A/A}$, developed normally until E12.5 when they displayed pallor of the liver
156 and were smaller (S1D Fig). After E13 no live *Mll1*$^{A/A}$ embryos were found (S1
157 Table). After FLP and Cre recombination, *Mll1*$^{FC/FC}$ embryos displayed the
158 same phenotype indicating that both A and FC are true null alleles in
159 concordance with the loss of MLL1 protein [40]. Furthermore the *Mll1*$^{A/A}$ and
160 *Mll1*$^{FC/FC}$ phenotype recapitulated another likely null allele [6] with all three
161 homozygous mice presenting the same embryonic lethality due to the failure
162 to engage definitive hematopoiesis [20].

163 To identify postnatal roles of MLL1, conditional mutagenesis using
164 *Rosa26-CreERT2* was applied to 2 month old adults. As expected, mice
165 lacking MLL1 developed severe bone marrow cytopenia and died or had to be
166 sacrificed on average within two weeks (Figs 1A and 1B). As previously
167 reported using the same conditional allele, *in vitro* deletion of *Mll1* in KSL-
168 enriched HSCs from *Mll1*$^{F/F;\ RC/+}$ mice resulted in significant downregulation of
169 *Hoxa9*, *Meis1*, *Mecom/Evi1* and *Prdm16* [6].

170 To bypass the bone marrow related lethality and thereby uncover non-
171 hematopoietic phenotypes, bone marrow from wild type (wt) B6.SJL mice was
172 transplanted into lethally irradiated *Mll1*$^{F/+;\ RC/+}$ or *Mll1*$^{F/F;\ RC/+}$ mice. After stable
173 engraftment tamoxifen gavage induced widespread Cre-mediated excision of

174 *Mll1* (Fig 1C). Examination of the bone marrow confirmed the successful and
175 near-complete reconstitution of the hematopoietic stem cell compartment by
176 wt donor cells. FACS analysis for KSL-Slam enriched hematopoietic stem
177 cells showed comparable frequencies in bone marrow transplanted (BMTx)
178 *Mll1*$^{FC/+;\ RC/+}$ and *Mll1*$^{FC/FC;\ RC/+}$ mice with the hematopoietic compartment
179 comprised only of wt cells of CD45.1 origin (Fig 1C). Notably, the BMTx
180 *Mll1*$^{FC/FC;\ RC/+}$ mice suffered from diarrhea and wasting (Fig 1D). These data
181 indicate that MLL1 is not only required in the hematopoietic compartment but
182 also elsewhere and this additional requirement is similarly critical for survival
183 as the hematopoietic requirement.

184 The small and large intestine harbor their stem cell compartments at
185 the base of the crypt. MLL1 is strongly expressed at the crypt bottom and in
186 the TA compartment whereas it is absent in differentiated cells above the TA
187 compartment (Figs 1E and S1E). RNA profiling of sorted ISCs and Paneth
188 cells confirmed expression of *Mll1* and the other family members in both cell
189 types however more strongly in ISCs (S1F Fig). In the mutant small intestine
190 of BMTx *Mll1*$^{FC/FC;\ RC/+}$ mice, expression of MLL1 was efficiently ablated (Fig
191 2A). Loss of stem cell markers olfactomedin (OLFM4) and SOX9 suggested
192 depletion of ISCs in the small intestine of BMTx *Mll1*$^{FC/FC;\ RC/+}$ mice (Fig 2A).
193 Consistent with this, the mutant showed decreased proliferation in the crypt as
194 demonstrated by strongly reduced expression of the mitotic marker Ki67 (Fig
195 2A). However, the intestinal epithelium of *Mll1*$^{FC/FC;\ RC/+}$ mice revealed no
196 apparent change in global H3K4 mono-, di- and trimethylation (S1G Fig).

197 Shortened villi with distorted morphology including vacuolar structures
198 at the tip indicated diminished replenishment of cells into the villus (Fig 2B).

199 Furthermore we observed increased numbers of enlarged goblet cells
200 distributed irregularly along the villus and also ectopically in the crypt (Fig 2B).
201 However, Paneth cells appeared unchanged possibly due to their longer life
202 span (Fig 2C). Similarly, as evaluated by chromogranin A and alkaline
203 phosphatase, the enteroendocrine and absorptive lineages appeared to be
204 unaffected (Fig 2C).

205 Without bone marrow rescue, *Mll1*$^{FC/FC;\ RC/+}$ mice showed the same
206 defects with depletion of ISCs, decreased proliferation and a distortion of the
207 secretory lineage (S2A-S2C Figs). Differentiation into the enteroendocrine
208 and absorptive lineage was also apparently unaffected (S2D Fig). Notably the
209 hallmark of Wnt signalling, nuclear β-catenin, was also unaffected (S2E Fig).

210

211 **Intestinal epithelium-specific *Mll1* conditional mutagenesis recapitulates**
212 **ubiquitous deletion**

213 To delete *Mll1* exclusively in the adult intestine we employed the
214 tamoxifen-inducible gut epithelium-specific *Villin-CreERT2* strain [41]. After
215 tamoxifen administration *Mll1*$^{FC/FC;\ Vil\text{-}CreERT2/+}$ mice lost weight compared to
216 control mice (Fig 3A). In agreement with our observations after ubiquitous
217 deletion of *Mll1,* OLFM4, SOX9 and proliferation were markedly decreased,
218 goblet cells were increased whereas Paneth and enteroendocrine cell
219 numbers were unchanged (Figs 3B and 3C).

220

221 **Transcriptome analysis identifies key intestine specific transcription**
222 **factors and *Jaml* as central to the crypt stem cell niche**

223 For transcriptome analysis, ISCs and Paneth cells were isolated 4 and

224 10 days after tamoxifen administration from *Mll1*$^{FC/+;\ Lgr5\text{-}eGFP\text{-}CreERT2/+}$ and
225 *Mll1*$^{FC/FC;\ Lgr5\text{-}eGFP\text{-}CreERT2/+}$ littermates (S3 Fig). Using 75 base-pair reads, 20-
226 37 million reads per sample with high levels of uniqueness (70-77% in Lgr5^{+}
227 ISCs and 60-76% in Paneth cells; S4A-S4C Figs) and comparable
228 mappability (99%) were obtained. Principal component analysis (PCA)
229 revealed that our datasets are in good agreement with published datasets
230 obtained from sorted ISCs and Paneth cells [35, 42] (S4D Fig).
231 We applied DESeq2 to analyze differentially expressed genes (DEGs).
232 For the 4 day Lgr5^{+} stem cell profile, only 87 and 49 genes were up- or
233 downregulated at a 5% false discovery rate (FDR) after removal of MLL1 (Fig
234 4A, Supplementary excel file 1). However, none of the upregulated transcripts
235 were increased by more than log2-fold and by DAVID analysis were mainly
236 related to diverse terms such as 'response to metal ion', 'organic acid
237 metabolic process' and 'regulation of lipid metabolic process' (Fig 4B). In
238 contrast the most significant terms associated with the downregulated mRNAs
239 were 'regulation of gene expression', 'epithelial cell differentiation' and 'cell
240 proliferation' (Fig 4B). The 10 day profile revealed 179 DEGs, of which 105
241 were upregulated, 74 were downregulated with significant overlaps to the 4
242 day profile (Supplementary excel file 1, Table 1).
243

244 **Table 1. Downregulated mRNAs common to both 4 and 10 day stem cell**
245 **profiles.**

Gene		4d C	KO	FC	10d C	KO	FC
Jaml/Amica1	Junction Adhesion Molecule Like	4124	119,9	**34,4**	3779	113,4	**33,3**
Pitx2	Paired Like Homeodomain 2	1399,6	162,9	**8,6**	854,8	34,7	**24,6**
Far1	FattyAcyl-CoA Reductase 1	402,3	229,1	**1,8**	231,8	47,4	**4,9**
Foxa1/ Hnf3α	Forkhead Box A1	356,8	105	**3,4**	428,4	93,9	**4,6**
Onecut2/ Hnf6β	Onecut Homeobox 2	2334,5	1177,1	**2,0**	2411,9	583	**4,1**
Gata4	GATA Binding Protein 4	676,4	356,9	**1,9**	508,2	136,7	**3,7**
Ces2g	Carboxyl esterase 2	275,2	177	**1,6**	209,9	58,6	**3,6**
Pla2g2a	Phospholipase A2 group IIA	291,3	119	**2,5**	215,7	68,2	**3,2**
Hspa8	Hsp 70 family	12104	4655,8	**2,6**	7654,5	25856	**3,0**
E230029C05	ncRNA	221,9	115,8	**1,9**	203,4	70,9	**2,9**
Casc4	Cancer Susceptible 4	120,5	61,4	**2,0**	255,1	93,9	**2,7**
Anpep	Alanyl amino peptidase N	855,8	562,5	**1,5**	393,1	150,8	**2,6**
Defa29	Defensinα 29	859,4	556,3	**1,5**	860,3	336,2	**2,6**
Lyz1	Lysozyme	10861	7181,7	**1,5**	8334,4	3429	**2,4**
Defa3	Defensinα 3	342,6	239,5	**1,4**	521,2	214,7	**2,4**
Lcp1	Lymphocyte Cytosolic P1	824,4	576	**1,4**	662	291	**2,3**
Defa35	Defensinα 35	831,4	555,4	**1,5**	938,4	431,4	**2,2**
Gm10925	pseudogene?	18872	14115	**1,3**	30453	14252	**2,1**
Afap1l1	Lnc-Afap1/1	485,5	354,5	**1,4**	420,6	197	**2,1**
Phlpp1	PH Domain Leucine Rich Phosphatase	468,7	302,8	**1,6**	480,5	227	**2,1**
Fap1	Familial Adenomatous Polyposis 1	990,5	768,4	**1,3**	1459,8	690,9	**2,1**
Casp6	Caspase 6	4727,6	3356,6	**1,4**	3861,6	1835	**2,1**
mt-Atp6	Mitochondrial encoded ATP Synthase S6	49048	40226	**1,2**	61873	29894	**2,1**
Fam149a	Toll-like receptor 3?	170,7	97,6	**1,8**	193,9	94,3	**2,1**
Zfpm1	FOG1 (Friend of Gata 1)	198,5	146	**1,4**	216,6	106,2	**2,0**

246 mRNAs expressed more than 150 reads in wt and downregulated more than 2
247 fold in the 10 day profile are shown. FC, fold change.
248

249 Gene set enrichment analysis (GSEA) of both 4 and 10 day ISC

250 profiles revealed that overall ISC signature genes were downregulated
251 whereas goblet cell signature genes were upregulated (Figs 4C-4G; S5A and
252 S5B Figs), which concords with our immunohistochemical analyses. We
253 focused on the overlap between the 4 and 10 day downregulated mRNAs.
254 The transcription factors *Pitx2, Foxa1*, *Onecut2* and *Gata4* are prominent
255 (Table 1; Fig 4E). The expression of *Foxa1* and *Pitx2* and was evaluated by
256 qRT-PCR and good agreement to the RNA-sequencing mRNA reads was
257 found (S5C Fig). These data suggest a role for MLL1 in maintaining the
258 transcriptional identity of ISCs.

259 However the top downregulated gene in both stem cell profiles (34.7
260 and 33.3 fold down) was junction adhesion molecule like (*Jaml* or *Amica1*;
261 Figs 4A, 4F, S5C) previously identified as an ISC signature gene [43, 44]. It is
262 highly expressed in Lgr5^{+} ISCs, where it appears to rely completely on MLL1,
263 but not in Paneth cells (at least 55 fold lower expressed in Paneth cells; S5D
264 Fig). JAML is a 65 kDa type I transmembrane glycoprotein in the JAM subset
265 of the immunoglobulin superfamily. JAML mediates adhesion of monocytes to
266 endothelial cells and neutrophil migration across epithelial cell monolayers
267 through interaction with Coxsackie and adenovirus receptor (CXADR or CAR)
268 in tight junctions [45]. However, the cognate receptor in the intestinal
269 epithelium is unknown. Notably the transcript for CAR-like soluble protein
270 (*Clsp*) (GM1123) is upregulated in both 4 and 10 day profiles (Supplementary
271 excel file 1). CLSP is closely related to CXADR however it lacks a
272 transmembrane domain [46].

273

274 **Loss of MLL1 in ISCs provokes transcriptional changes in Paneth cells**

275 ISCs are anchored in the crypt in close association with Paneth cells.
276 In order to elucidate whether the transcriptional changes in ISCs influenced
277 the neighboring Paneth cells, we also analyzed Paneth cell transcriptional
278 profiles 4 days after deletion of *Mll1* in Lgr5^{+} ISCs, with 198 and 72 transcripts
279 up- and downregulated respectively (Fig 5A, Supplementary excel file 1). The
280 most significant terms associated with downregulated mRNAs relate to
281 perturbation of protein folding and homeostasis in the endoplasmic reticulum
282 (Figs 5B-5D). In contrast upregulated mRNAs associate with metabolic
283 changes. Strikingly, transcripts of genes belonging to all five of the respiratory
284 chain complexes were upregulated (Figs 5B-5D). Paneth cells normally run on
285 glycolysis with lactate as the end product whereas ISCs depend on
286 mitochondrial oxidative phosphorylation [47]. These transcriptional changes
287 suggest that loss of MLL1 in the stem cell compartment provokes changes in
288 Paneth cells and indeed expression of Paneth cell marker genes was
289 downregulated (Figs 5C and 5D).

290 **Skewed differentiation of organoids after loss of MLL1**

291 To evaluate the cell-intrinsic requirement of MLL1 in the small intestine,
292 we isolated crypts from *Mll1*$^{F/+;\ RC/+}$ and *Mll1*$^{F/F;\ RC/+}$ mice and cultured them to
293 form organoids. After passaging, organoids were induced with 4-OH
294 tamoxifen for 24 hours on day 2. After further passages, the *Mll1*$^{FC/FC;\ RC/+}$
295 organoids increasingly formed round, less differentiated cyst-like spheres
296 (Figs 6A-6C). qRT-PCR revealed mRNA downregulation of *Jaml* and
297 transcription factors such as *Pitx2 and Foxa1* (Fig 6D) indicating the expected
298 loss of ISCs and elevation of the goblet cell marker, *Muc2*. Notably the cyst-
299 like organoids kept proliferating after loss of MLL1 and the Lgr5^{+} ISC marker,

300 *Olfm4,* was elevated indicating differences between events in the crypt and in
301 culture. Differences are also indicated by the elevation of the Paneth cell
302 markers *Mmp7*, *Wnt3* and the elevation of the putative JAML receptor, *Cxadr*,
303 which might enable the transition from organoids to spheroids (Fig 6D). These
304 data establish a cell intrinsic requirement for MLL1 and indicate that it is
305 required to maintain ISCs in organoid cultures.

306 ## Discussion

307

308 Here we add a fourth stem cell to the known MLL1 repertoire of (i)
309 HSCs [20, 21], (ii) skeletal muscle satellite cells [26] and (iii) postnatal neural
310 stem cells (NSCs) [27]. The complete concordance between known MLL1
311 functions in postnatal stem cells suggests that MLL1 conveys an essential
312 stem cell property. This possibility is enhanced by comparison to the MLL1
313 paralogue, MLL2, whose known functions in adult mice do not relate to stem
314 cells rather macrophages (to respond to lipopolysaccharides) or fertility [48-
315 51].

316 To explore the idea that MLL1 conveys a key stem cell property, we
317 inspected the transcriptome profiles after conditional loss of MLL1 in the four
318 adult/postnatal stem cells [26, 27, 52] (Supplementary excel file 1). However
319 no shared candidate regulators or gene expression programs were identified.
320 Although deeper, more systematic, transcriptome or cell biology approaches
321 may reveal a shared MLL1 stem cell property, the lack of concordance
322 between MLL1 regulation of these four stem cell transcriptomes is not
323 unexpected. Previous work with MLL1 noted that direct target genes are not
324 shared between different cell types [52] and a similar observation was made
325 for MLL2 [48]. That is, the regulation of gene expression by the Trithorax
326 homologues, MLL1 and MLL2, varies depending on the cell type and is not
327 universal.

328 As again documented here for ISCs, the strongest relationship
329 between the loss of MLL1 and cellular processes involves the downregulation
330 of mRNAs that regulate transcription. Upon loss of MLL1, downregulation of

331 transcription factor mRNAs include - (i) in HSCs; *Mecom, Prdm16, Pbx1,*
332 *Eya1, Meis1* and *Hoxa9*; (ii) in postnatal NSCs; *Nkx2.1, Nkx2.3*; (iii) in satellite
333 cells; *Pax7* and (iv) in ISCs; *Pitx2, Foxa1, Gata4* and *Onecut2*.

334 How does MLL1 regulate key lineage specific transcription factors
335 differently in different lineages? MLL1 and MLL2 are amongst the few proteins
336 that include the CxxC zinc finger that binds unmethylated CpG dinucleotides
337 [23, 53] as well as a PHD finger that binds H3K4me3 [54]. Hence, as
338 suggested before [48], MLL1 and 2 have the potential ability to bind CpG
339 island promoters without the need for recruitment by sequence specific DNA
340 binding transcription factors. This potential accords with the observation that
341 both MLL1 and 2 appear to be bound at almost all active promoters [40, 55].
342 Consequently additional factors are required to explain the restricted
343 transcriptional specificities of the MLLs. Notable in this regard, PAX7 is bound
344 to MLL1 when satellite cells are activated, and enhanced transcriptional
345 activation from both the *Myf5* promoter, to initiate skeletal muscle
346 replenishment, and the *Pax7* promoter itself, depends on MLL1 [26]. This
347 suggests that key transcription factors can either acquire the ability to interact
348 with MLL1 bound at target promoters or recruit MLL1 to target promoters, or
349 both.

350 Amongst the transcription factor mRNAs identified after loss of MLL1 in
351 ISCs, *Pitx2* is prominent. *Pitx2* was previously identified as a direct target of
352 MLL1 in ESCs and HSCs/hematopoietic progenitor cells [56, 57]. PITX2 is a
353 homeodomain protein responsible for left-right asymmetric morphogenesis in
354 the gut and proper positioning of the small intestine in the body cavity [58].
355 Also notably identified in ISCs are *Foxa1* and *Onecut2*. Both genes,

356 previously known as *Hnf3*α and *Hnf6*α, are expressed in all epithelia of the
357 gastrointestinal tract from its embryonic origin into adulthood. Together with
358 *Math1*, they are critical for goblet cell differentiation and function [59, 60].
359 *Gata4*, which has previously been described as an MLL1 target gene [61], is
360 also amongst the top downregulated mRNAs after loss of MLL1. Some
361 aspects of the intestine specific deletion of *Gata4* in the adult mouse resemble
362 the MLL1 phenotype described here including decreased proliferation in the
363 crypts with increased numbers of goblet cells [62].

364 In addition to the central relationship between MLL1 and transcription
365 factor expression, by far the most dramatically downregulated mRNA in both 4
366 and 10 day ISC transcriptomes was *Jaml*, which was previously included in
367 the transcriptome profile that characterizes ISCs [43, 44]. As a prominent cell
368 adhesion molecule, investigations by Tetteh and Clevers found that *Jaml* is
369 expressed in the base of the crypt in ISCs but not Paneth cells and used
370 *Villin-CreERT2* to conditionally knock it out [63]. Loss of *Jaml* resulted in loss
371 of both *Olfm4*$^{+}$ ISCs and proliferation in the crypt without loss of Paneth cells.
372 These observations support the conclusion that MLL1 contributes to ISC
373 function mainly by expression of *Jaml*. However in contrast to the loss of
374 MLL1, Tetteh and Clevers did not observe an increase in goblet cells after
375 loss of JAML. Imbalanced commitment in the secretory lineage may indicate a
376 second aspect of MLL1 function that does not operate through *Jaml*
377 expression, possibly including the regulation of *Gata4* expression [62] and
378 other transcription factors. Upon loss of MLL1 *Jaml* is downregulated and the
379 close association between stem cells and Paneth cells is probably
380 destabilized (Fig 7). ISCs are anchored in the crypt surrounded by Paneth

381 cells, which confers positional identity. The central ISC at the bottom of the
382 crypt flanked by two Paneth cells has long-term self-renewal potential
383 compared to border ISCs [64]. Interestingly positional identity of NSCs seems
384 to be regulated in an MLL1 dependent fashion [27].

385 Once again we report the remarkably specific dependency of the
386 expression of one or two genes on a Trithorax homologue. As described here,
387 loss of MLL1 resulted in loss of *Jaml* expression with subsequent significant
388 functional consequences in the crypt. In ESCs, the expression of one gene,
389 *Magoh2*, entirely depends on MLL2. Removal of MLL2 resulted in the
390 suppression of *Magoh2* expression by H3K27 methylation, followed by DNA
391 methylation [48], thereby providing more evidence supporting the conclusion
392 that a primary function of Trithorax action is to prevent Polycomb-Group
393 repression [65]. These observations and conclusions with *Magoh2* in ESCs
394 were recently confirmed [66]. Selective gene specific anti-repression could
395 also explain the action of MLL2 on *Pigp* in macrophages [49] and MLL1 on
396 *Hoxa9* in HSCs [25].

397 Despite a high degree of evolutionary conservation and near-
398 ubiquitous expression, the Trithorax homologues appear to regulate a small
399 number of genes in cell-type specific patterns, one or two of which are entirely
400 dependent on one homologue for expression due to anti-repression. In ISCs
401 this extraordinary specificity is focused on *Jaml* with functional consequences
402 for the crypt niche. As observed in other adult stem cells, MLL1 also regulates
403 the expression of transcription factors in ISCs that likely influence lineage
404 commitment decisions. These observations lead to the attractive proposition
405 that MLL1 is a master stem cell regulator. However a unifying molecular basis

406 for this proposition remains to be identified.

407 ## Methods and materials

408

409 **Targeting constructs**

410 The targeting construct for *Mll1* was generated using recombineering (S1A
411 Fig) employing an engrailed-intron-splice-acceptor-IRES-LacZ-Neomycin-
412 polyA cassette flanked by FRT sites [39]. The critical exon 2, which upon
413 deletion results in a frameshift and a premature stop codon in exon 3, was
414 flanked by loxP sites.

415 **Gene targeting and generation of conditional knockout mice**

416 Gene targeting in R1 embryonic stem cells (ESCs) was performed as
417 described [67]. Correct integration in the *Mll1* locus was confirmed by
418 Southern blot analysis using an internal probe and 5' and 3' external probes
419 (S1B and S1C Figs). Two correctly targeted ESC clones were injected into
420 blastocysts and gave rise to several chimeras, which were able to establish
421 germ line transmission. *Mll1*$^{A/+}$ mice were crossed to the *hACTB-Flpe* line to
422 generate *Mll1*$^{F/+}$ mice. *Mll1*$^{A/+}$ and *Mll1*$^{F/+}$ mice were backcrossed at least six
423 generations to *C57BL/6JOlaHsd* mice. Subsequently, those mice were
424 crossed to the *Rosa26-Cre-ERT2* (*RC*) line [5] to generate conditional,
425 tamoxifen-inducible *Mll1*$^{F/+;\ RC/+}$ mice. *Mll1*$^{F/+}$ mice were bred with *Lgr5-eGFP-*
426 *CreERT2* and *Villin-CreER*^{T2} (*Vil-Cre-ERT2*) [29, 41] mice. Primers for
427 genotyping are provided in S2 Table. Experiments were performed in
428 accordance with German animal welfare legislation, and were approved by
429 the relevant authorities, the Landesdirektion Dresden.

430 **Tamoxifen**

431 Tamoxifen (Sigma Aldrich, T5648) was given to at least 10-week old mice by

432 gavage (4.5 mg per day) for six days with three days break in between [68].
433 For RNA-Sequencing experiments, *Mll1*$^{F/+;}$ and *Mll1*$^{F/F;\ Lgr5\text{-}eGFP\text{-}CreERT2/+}$ mice
434 received 1 mg tamoxifen via intraperitoneal (IP) injection for 3 consecutive
435 days. Intestinal organoids were induced on day 2 after splitting using 800 nM
436 4-OH tamoxifen (Sigma H7904) for 24 h.

437 **Bone marrow transplantation**

438 *Mll1*$^{F/+;\ RC/+}$ and *Mll1*$^{F/F;\ RC/+}$ recipient (CD45.2) mice were lethally irradiated
439 with 8.5 Gy (X-ray source MaxiShot from Yxlon). Bone marrow cells from
440 B6.SJL mice (CD45.1) were prepared by crushing with a mortar and pestle in
441 ice-cold PBS supplemented with 5% fetal bovine serum. Red blood cells were
442 removed with ACK lysis buffer (Thermo Fisher Scientific). 1 x 10^6 lineage
443 depleted (Lin^-) bone marrow cells were injected into the retro-orbital venous
444 plexus. Animals were maintained on water containing 1,17 mg/ml Neomycin
445 (Merck) for three weeks after irradiation. Complete donor cell engraftment of
446 wt $CD45.1^+$ cells was confirmed by flow cytometry on peripheral blood with
447 antibodies directed against the following murine antigens (clones given in
448 brackets): CD45.1 (A20), CD45.2 (104), CD11b (M1/70), Gr-1 (RB6-8C5).
449 Stably engrafted mice were fed six times with tamoxifen 30 weeks after
450 transplantation. FACS analysis for KSL-Slam enriched HSCs was done with
451 antibodies directed against the following murine antigens: CD3 (2C11; 17A2),
452 CD11b (M1/70), CD16/32 (93), CD19 (eBio 1D3), CD34 (RAM34), CD45.1
453 (A20), CD45.2 (104), CD45R (RA3-6B2), CD117 (2B8), CD135 (A2F10), Gr-1
454 (RB6-8C5), Nk1.1 (PK136), Ter119 (Ter119, all eBioscience), CD11b (M1/70)
455 and CD45.1 (A20, all BD Pharmingen), Sca-1 (D7), CD48 (HM48-1) and
456 CD150 (TC15-12F1, all BioLegends). Lin^- cells were identified by lack of CD3,

457 CD11b, CD19, CD45R, Gr-1, Nk1.1 and Ter119 expression.

458 **5-Bromo-2-deoxyuridine (BrdU) assay**

459 Mice were injected IP with BrdU (0.6 mg/10 g body weight in sterile PBS) and
460 sacrificed 2 h later. The jejunum was dissected in cold PBS and processed for
461 immunohistochemistry.

462 **Histochemistry and immunohistochemistry**

463 Mouse intestine was flushed gently with cold PBS. Embryos were dissected
464 from plugged mice on the respective gestational stage and placed in PBS.
465 Intestine and embryos were fixed in 4% paraformaldehyde overnight.
466 Dehydration and paraffin infiltration utilized the Paraffin-Infiltration-Processor
467 (STP 420, Zeiss). Dehydrated tissues were embedded in paraffin (Paraffin
468 Embedding Center EG1160, Leica) and 5 µm sections were prepared.
469 Sections were deparaffinized in xylene, rehydrated through a series of
470 alcohols, stained, dehydrated, and mounted. Femur sections were stained
471 with Giemsa according to standard protocols. For the basic evaluation of the
472 intestine hematoxylin and eosin (H&E) stain was performed. Periodic acid-
473 Schiff (PAS) stain and alcian blue were used to identify goblet cells. For
474 enterocytes, alkaline phosphatase stain was performed using two different
475 methods. Sections were either incubated with Red Alkaline Phosphatase
476 Substrate (Vector red, Vector Laboratories) for 10 minutes (min) or with
477 nitroblue tetrazolium/5-bromo-4-chloro-3-indolyl phosphate solution for 30 min
478 at room temperature (RT). For immunohistochemistry, antigen retrieval was
479 performed by microwaving slides in 10 mM citrate buffer (pH 6.0) for 12 min
480 (Microwave RHS 30, Diapath). Endogenous peroxidases were quenched with
481 0.3% H_2O_2 in methanol. Sections were incubated in blocking serum (5% goat

482 serum) for 1 hr at RT followed by overnight incubation with primary antibodies
483 (S3 Table) at 4°C. Following incubation with the secondary antibody (S3
484 Table) the immune peroxidase was detected using a Vectastain ELITE ABC
485 kit (Vector) and visualized with a solution of diaminobenzidine (Sigma Aldrich)
486 in the presence of 0.01% H_2O_2. All sections were counterstained with
487 hematoxylin or alcian blue. Images were collected with an Olympus WF
488 upright microscope and analyzed using the MetaMorph® Microscopy
489 Automation and Image Analysis Software.

490 ***In situ* hybridization**

491 The protocol for *in situ* hybridization was modified from [69]. Briefly, 8 µm
492 thick sections were rehydrated. The sections were treated with 0.1 N HCl and
493 proteinase K. Slides were postfixed and sections were then demethylated with
494 acetic anhydride and prehybridized. Hybridization was done with 2 µg/ml
495 digoxigenin (DIG)-labeled *Olfm4* RNA probe for 24 h at 65°C. Slides were
496 washed and incubated with blocking solution for 1 hr. The sections were
497 incubated with anti-DIG-alkaline phosphatase conjugate overnight at 4°C.
498 Slides were washed and developed with BM purple.

499 **Crypt isolation**

500 The jejunum was harvested from mice, flushed with ice cold PBS to remove
501 any faecal content and cut open longitudinally. The tissue was placed lumen
502 side up on a petri dish and the villi were removed by gently scraping the tissue
503 using a glass cover slip. The tissue was cut into 2-4 cm pieces and was
504 washed several times with ice-cold PBS to remove residual villi fragments.
505 Tissues were transferred into a fresh tube containing 15 ml of 2 mM
506 EDTA/PBS chelation buffer and placed on a rotating wheel for 30 min at 4°C.

507 The crypts were then detached from the basal membrane by vigorous shaking
508 in 5% FCS/PBS solution. The suspension was filtered with a 100 µm cell
509 strainer followed by a 70 µm cell strainer. Isolated crypts were centrifuged at
510 800 rpm for 5 min at 4°C. The final fraction consisted of pure crypts and was
511 used for cell culture or single cell dissociation.

512 **Organoid culture**

513 Purified crypts were resuspended in 10 ml DMEM/F12 (Life Technologies). 10
514 µl of the crypt suspension was used to count the number of crypts under the
515 microscope. The pelleted crypts were resuspended in Matrigel® matrix
516 (Corning) at desired crypt density. Approximately, 400 crypts in 25 µl
517 Matrigel® matrix were seeded per well in a pre-warmed 24-well plate and
518 incubated for 15 min at 37°C until the Matrigel® matrix solidified. Then, 400 µl
519 of IntestiCult™ Organoid Growth Medium (STEMCELL Technologies) was
520 added to each well. Organoids were cultured at 37°C in a 5% CO_2 incubator
521 and maintained in culture for 5 days before being passaged and split for
522 experimental procedures. The growth medium was replaced every 2-3 days

523 **Flow cytometry**

524 ISCs were initially characterized and identified with the use of an *Lgr5-eGFP-*
525 *CreERT2* knockin allele [29]. *Mll1*$^{F/+}$ and *Mll1*$^{F/F;\ Lgr5\text{-}eGFP\text{-}CreERT2/+}$ littermates
526 (n=4) were given tamoxifen via IP injections for 3 consecutive days and were
527 dissected 4 and 10 days later. Crypts were dissociated into single cells with
528 TrypLE Express (Thermo Fisher Scientific) for 30 min at 37°C. Dissociated
529 cells were passed through 70 µm cell strainer and washed with 5% FCS/PBS.
530 Cells were stained with antibodies with the following antibodies for 45 min on
531 ice: anti-mouse CD24 PE (clone M1/69), anti-mouse CD326 (EpCAM) APC

532 (clone G8.8), anti-mouse CD45 Alexa-Fluor 700 (clone 104). Sorting was
533 performed on a FACS Aria^{TM} III cell sorter (BD). After scatter discrimination to
534 remove doublets the cell suspension was negatively selected with SYTOX
535 blue dead cell stain and anti-CD45 to remove dead and hematopoietic cells,
536 respectively. The cells where then positively selected with anti-EpCAM to
537 enrich for intestinal epithelial cells. According to [70] CD45^{-}, EpCAM^{high},
538 CD24^{med} and GFP^{high} characterized ISCs and CD45^{-}, EpCAM^{high}, CD24^{high}
539 and GFP^{-} characterized Paneth cells (S3A and S3B Figs). *Mll1* recombination
540 via PCR on the sorted populations confirmed deletion of *Mll1* solely in the
541 stem cell compartment (S3C Fig).

542 **RNA sequencing**

543 300 intestinal stem and Paneth cells were sorted into 2 µl of nuclease free
544 water with 0.2% Triton-X 100 and 4 U murine RNase Inhibitor (NEB). RNA
545 was reverse transcribed (Invitrogen) and cDNA amplified using Kapa HiFi
546 HotStart Readymix (Roche). The cDNA quality and concentration was
547 determined with the Fragment Analyzer (Agilent). Samples were subjected to
548 library preparation (TruePrep DNA library Prep Kit V2 for Illumina, Vazyme).
549 Libraries were purified followed by Illumina sequencing on a Nextseq500 with
550 a sample sequencing depth of 30 million reads on average. The short reads
551 were aligned to the mm10 transcriptome with GSNAP (2018-07-04) and a
552 table of read counts per gene was created based on the overlap of the
553 uniquely mapped reads with the Ensembl Gene annotation version 92, using
554 featureCounts (version 1.6.3). Normalization of the raw read counts based on
555 the library size and testing for differential gene expression between the
556 different genotypes was performed using the DESeq2 R package (version

557 1.24.0). Genes with an adjusted p-value (padj)≤ 0.05 were considered as
558 significantly differentially expressed accepting a 5% FDR. To identify
559 enrichment for particular biological processes and pathways associated with
560 the DEGs, the DAVID GO/BP/FAT and KEGG database [71] was used. Gene
561 set enrichment analysis was performed using GSEA software from the Broad
562 Institute [72].

563 **Reverse transcription and quantitative PCR (qRT-PCR) analysis**

564 RNA from sorted cells and organoids was extracted using Trizol (Sigma-
565 Aldrich) and reverse transcribed using AffinityScript Multiple Temperature
566 cDNA Synthesis Kit (Agilent Technologies). Real-time quantitative PCR was
567 performed with GoTaq qPCR Master Mix (Promega) by Mx3000P QPCR
568 System (Agilent Technologies). Ct values were normalized against *Rpl19*.
569 Primer sequences and length of the amplified products are given in S2 Table.
570 Fold differences in expression levels were calculated according to the $2^{-\Delta Ct}$
571 method [73].

572 **Quantification and Statistical analysis**

573 Data is presented as mean and error bars indicate standard deviation (s.d.)
574 unless otherwise indicated. Statistical details of the experiments can be found
575 in the figure legends. Graphs and statistics were generated with GraphPad
576 Prism software (v6.0) and Microsoft excel. Significance (p-values) for Kaplan-
577 Meier graphs was determined by Mantel-Cox test. Significance (p-values <
578 0.05) was determined with Wald test or two-tailed Student's *t* test.
579 Significance for the breeding statistics was determined with Chi-square test. N
580 indicates the numbers of independent biological replicates per experiment
581 unless otherwise indicated.

582 **Data availability**: RNA sequencing data have been deposited in the Gene
583 Expression Omnibus under accession number GSE 157285.

584

585 ## Acknowledgements

586 We thank Mandy Obst, Isabell Kolbe, Heike Petzold and Stefanie
587 Weidlich for excellent technical assistance. We also thank the Biomedical
588 Services (BMS) of the Max Planck Institute of Molecular Cell Biology and
589 Genetics, Dresden for the excellent service and technical assistance. We are
590 grateful to Prof. Sebastian Zeissig (CRTD, Dresden) for helpful advice. We
591 thank the core facilities of the Biotechnology Center for providing assistance
592 with flow cytometry (Katja Schneider). The Advanced Imaging Facility, a core
593 facility of the CMCB Technology Platform at TU Dresden, http://biotp.tu-
594 dresden.de/facilities/advanced-imaging/ assisted this research.

References

1. Blanpain C, Fuchs E. Stem cell plasticity. Plasticity of epithelial stem cells in tissue regeneration. Science. 2014;344(6189):1242281. Epub 2014/06/14. doi: 10.1126/science.1242281. PubMed PMID: 24926024; PubMed Central PMCID: PMCPMC4523269.
2. Simons BD, Clevers H. Strategies for homeostatic stem cell self-renewal in adult tissues. Cell. 2011;145(6):851-62. doi: 10.1016/j.cell.2011.05.033. PubMed PMID: 21663791.
3. Stadhouders R, Filion GJ, Graf T. Transcription factors and 3D genome conformation in cell-fate decisions. Nature. 2019;569(7756):345-54. Epub 2019/05/17. doi: 10.1038/s41586-019-1182-7. PubMed PMID: 31092938.
4. Arndt K, Kranz A, Fohgrub J, Jolly A, Bledau AS, Di Virgilio M, et al. SETD1A protects HSCs from activation-induced functional decline in vivo. Blood. 2018;131(12):1311-24. Epub 2018/01/20. doi: 10.1182/blood-2017-09-806844. PubMed PMID: 29348130.
5. Schmidt K, Zhang Q, Tasdogan A, Petzold A, Dahl A, Arneth BM, et al. The H3K4 methyltransferase Setd1b is essential for hematopoietic stem and progenitor cell homeostasis in mice. Elife. 2018;7. Epub 2018/06/20. doi: 10.7554/eLife.27157. PubMed PMID: 29916805; PubMed Central PMCID: PMCPMC6025962.
6. Chen Y, Anastassiadis K, Kranz A, Stewart AF, Arndt K, Waskow C, et al. MLL2, Not MLL1, Plays a Major Role in Sustaining MLL-Rearranged Acute Myeloid Leukemia. Cancer Cell. 2017;31(6):755-70 e6. Epub 2017/06/14. doi: 10.1016/j.ccell.2017.05.002. PubMed PMID: 28609655; PubMed Central PMCID: PMCPMC5598468.
7. Di Carlo V, Mocavini I, Di Croce L. Polycomb complexes in normal and malignant hematopoiesis. J Cell Biol. 2019;218(1):55-69. Epub 2018/10/21. doi: 10.1083/jcb.201808028. PubMed PMID: 30341152; PubMed Central PMCID: PMCPMC6314559.
8. Lyko F. The DNA methyltransferase family: a versatile toolkit for epigenetic regulation. Nat Rev Genet. 2018;19(2):81-92. Epub 2017/10/17. doi: 10.1038/nrg.2017.80. PubMed PMID: 29033456.
9. Piunti A, Shilatifard A. Epigenetic balance of gene expression by Polycomb and COMPASS families. Science. 2016;352(6290):aad9780. Epub 2016/06/04. doi: 10.1126/science.aad9780. PubMed PMID: 27257261.
10. Liang G, Lin JC, Wei V, Yoo C, Cheng JC, Nguyen CT, et al. Distinct localization of histone H3 acetylation and H3-K4 methylation to the transcription start sites in the human genome. Proc Natl Acad Sci U S A. 2004;101(19):7357-62. Epub 2004/05/05. doi: 10.1073/pnas.0401866101. PubMed PMID: 15123803; PubMed Central PMCID: PMCPMC409923.
11. Soares LM, He PC, Chun Y, Suh H, Kim T, Buratowski S. Determinants of Histone H3K4 Methylation Patterns. Mol Cell. 2017;68(4):773-85 e6. Epub 2017/11/14. doi: 10.1016/j.molcel.2017.10.013. PubMed PMID: 29129639; PubMed Central PMCID: PMCPMC5706784.
12. Choudhury R, Singh S, Arumugam S, Roguev A, Stewart AF. The Set1 complex is dimeric and acts with Jhd2 demethylation to convey symmetrical H3K4 trimethylation. Genes Dev. 2019;33(9-10):550-64. Epub 2019/03/08. doi: 10.1101/gad.322222.118. PubMed PMID: 30842216; PubMed Central PMCID: PMCPMC6499330.

13. Suganuma T, Workman JL. Chromatin and signaling. Curr Opin Cell Biol. 2013;25(3):322-6. doi: 10.1016/j.ceb.2013.02.016. PubMed PMID: 23498660.
14. Heintzman ND, Hon GC, Hawkins RD, Kheradpour P, Stark A, Harp LF, et al. Histone modifications at human enhancers reflect global cell-type-specific gene expression. Nature. 2009;459(7243):108-12. doi: 10.1038/nature07829. PubMed PMID: 19295514; PubMed Central PMCID: PMC2910248.
15. Ernst P, Vakoc CR. WRAD: enabler of the SET1-family of H3K4 methyltransferases. Brief Funct Genomics. 2012;11(3):217-26. Epub 2012/06/02. doi: 10.1093/bfgp/els017. PubMed PMID: 22652693; PubMed Central PMCID: PMCPMC3388306.
16. Roguev A, Schaft D, Shevchenko A, Pijnappel WW, Wilm M, Aasland R, et al. The Saccharomyces cerevisiae Set1 complex includes an Ash2 homologue and methylates histone 3 lysine 4. EMBO J. 2001;20(24):7137-48. Epub 2001/12/18. doi: 10.1093/emboj/20.24.7137. PubMed PMID: 11742990; PubMed Central PMCID: PMCPMC125774.
17. Milne TA, Briggs SD, Brock HW, Martin ME, Gibbs D, Allis CD, et al. MLL targets SET domain methyltransferase activity to Hox gene promoters. Mol Cell. 2002;10(5):1107-17. Epub 2002/11/28. doi: 10.1016/s1097-2765(02)00741-4. PubMed PMID: 12453418.
18. Yagi H, Deguchi K, Aono A, Tani Y, Kishimoto T, Komori T. Growth disturbance in fetal liver hematopoiesis of Mll-mutant mice. Blood. 1998;92(1):108-17. Epub 1998/06/25. PubMed PMID: 9639506.
19. Ernst P, Fisher JK, Avery W, Wade S, Foy D, Korsmeyer SJ. Definitive hematopoiesis requires the mixed-lineage leukemia gene. Dev Cell. 2004;6(3):437-43. Epub 2004/03/20. PubMed PMID: 15030765.
20. Jude CD, Climer L, Xu D, Artinger E, Fisher JK, Ernst P. Unique and independent roles for MLL in adult hematopoietic stem cells and progenitors. Cell Stem Cell. 2007;1(3):324-37. doi: 10.1016/j.stem.2007.05.019. PubMed PMID: 18371366; PubMed Central PMCID: PMC2234224.
21. Gan T, Jude CD, Zaffuto K, Ernst P. Developmentally induced Mll1 loss reveals defects in postnatal haematopoiesis. Leukemia. 2010;24(10):1732-41. doi: 10.1038/leu.2010.171. PubMed PMID: 20724987; PubMed Central PMCID: PMC2954260.
22. Slany RK. The molecular biology of mixed lineage leukemia. Haematologica. 2009;94(7):984-93. doi: 10.3324/haematol.2008.002436. PubMed PMID: 19535349; PubMed Central PMCID: PMC2704309.
23. Bach C, Mueller D, Buhl S, Garcia-Cuellar MP, Slany RK. Alterations of the CxxC domain preclude oncogenic activation of mixed-lineage leukemia 2. Oncogene. 2009;28(6):815-23. doi: 10.1038/onc.2008.443. PubMed PMID: 19060922.
24. Slany RK. MLL fusion proteins and transcriptional control. Biochim Biophys Acta Gene Regul Mech. 2020;1863(3):194503. Epub 2020/02/18. doi: 10.1016/j.bbagrm.2020.194503. PubMed PMID: 32061883.
25. Milne TA, Kim J, Wang GG, Stadler SC, Basrur V, Whitcomb SJ, et al. Multiple interactions recruit MLL1 and MLL1 fusion proteins to the HOXA9 locus in leukemogenesis. Mol Cell. 2010;38(6):853-63. doi: 10.1016/j.molcel.2010.05.011. PubMed PMID: 20541448; PubMed Central PMCID: PMC2902588.

26. Addicks GC, Brun CE, Sincennes MC, Saber J, Porter CJ, Francis Stewart A, et al. MLL1 is required for PAX7 expression and satellite cell self-renewal in mice. Nat Commun. 2019;10(1):4256. Epub 2019/09/20. doi: 10.1038/s41467-019-12086-9. PubMed PMID: 31534153; PubMed Central PMCID: PMCPMC6751293.
27. Delgado RN, Mansky B, Ahanger SH, Lu C, Andersen RE, Dou Y, et al. Maintenance of neural stem cell positional identity by mixed-lineage leukemia 1. Science. 2020;368(6486):48-53. Epub 2020/04/04. doi: 10.1126/science.aba5960. PubMed PMID: 32241942.
28. Clevers H. The intestinal crypt, a prototype stem cell compartment. Cell. 2013;154(2):274-84. doi: 10.1016/j.cell.2013.07.004. PubMed PMID: 23870119.
29. Barker N, van Es JH, Kuipers J, Kujala P, van den Born M, Cozijnsen M, et al. Identification of stem cells in small intestine and colon by marker gene Lgr5. Nature. 2007;449(7165):1003-7. Epub 2007/10/16. doi: 10.1038/nature06196. PubMed PMID: 17934449.
30. Gehart H, Clevers H. Tales from the crypt: new insights into intestinal stem cells. Nat Rev Gastroenterol Hepatol. 2019;16(1):19-34. Epub 2018/11/16. doi: 10.1038/s41575-018-0081-y. PubMed PMID: 30429586.
31. Tian H, Biehs B, Warming S, Leong KG, Rangell L, Klein OD, et al. A reserve stem cell population in small intestine renders Lgr5-positive cells dispensable. Nature. 2011;478(7368):255-9. doi: 10.1038/nature10408. PubMed PMID: 21927002; PubMed Central PMCID: PMC4251967.
32. Tetteh PW, Basak O, Farin HF, Wiebrands K, Kretzschmar K, Begthel H, et al. Replacement of Lost Lgr5-Positive Stem Cells through Plasticity of Their Enterocyte-Lineage Daughters. Cell Stem Cell. 2016;18(2):203-13. Epub 2016/02/03. doi: 10.1016/j.stem.2016.01.001. PubMed PMID: 26831517.
33. van Es JH, Sato T, van de Wetering M, Lyubimova A, Yee Nee AN, Gregorieff A, et al. Dll1+ secretory progenitor cells revert to stem cells upon crypt damage. Nat Cell Biol. 2012;14(10):1099-104. Epub 2012/09/25. doi: 10.1038/ncb2581. PubMed PMID: 23000963; PubMed Central PMCID: PMCPMC3789123.
34. Jadhav U, Saxena M, O'Neill NK, Saadatpour A, Yuan GC, Herbert Z, et al. Dynamic Reorganization of Chromatin Accessibility Signatures during Dedifferentiation of Secretory Precursors into Lgr5+ Intestinal Stem Cells. Cell Stem Cell. 2017;21(1):65-77 e5. Epub 2017/06/27. doi: 10.1016/j.stem.2017.05.001. PubMed PMID: 28648363; PubMed Central PMCID: PMCPMC5505276.
35. Yu S, Tong K, Zhao Y, Balasubramanian I, Yap GS, Ferraris RP, et al. Paneth Cell Multipotency Induced by Notch Activation following Injury. Cell Stem Cell. 2018;23(1):46-59 e5. Epub 2018/06/12. doi: 10.1016/j.stem.2018.05.002. PubMed PMID: 29887318; PubMed Central PMCID: PMCPMC6035085.
36. Yang W, Ernst P. Distinct functions of histone H3, lysine 4 methyltransferases in normal and malignant hematopoiesis. Curr Opin Hematol. 2017;24(4):322-8. Epub 2017/04/05. doi: 10.1097/moh.0000000000000346. PubMed PMID: 28375985; PubMed Central PMCID: PMCPMC5603181.

744 37. Tetteh PW, Farin HF, Clevers H. Plasticity within stem cell hierarchies
745 in mammalian epithelia. Trends Cell Biol. 2015;25(2):100-8. doi:
746 10.1016/j.tcb.2014.09.003. PubMed PMID: 25308311.
747 38. Fu J, Teucher M, Anastassiadis K, Skarnes W, Stewart AF. A
748 recombineering pipeline to make conditional targeting constructs. Methods
749 Enzymol. 2010;477:125-44. Epub 2010/08/12. doi: 10.1016/s0076-
750 6879(10)77008-7. PubMed PMID: 20699140.
751 39. Testa G, Schaft J, van der Hoeven F, Glaser S, Anastassiadis K,
752 Zhang Y, et al. A reliable lacZ expression reporter cassette for multipurpose,
753 knockout-first alleles. Genesis. 2004;38(3):151-8. doi: 10.1002/gene.20012.
754 PubMed PMID: 15048813.
755 40. Denissov S, Hofemeister H, Marks H, Kranz A, Ciotta G, Singh S, et al.
756 Mll2 is required for H3K4 trimethylation on bivalent promoters in embryonic
757 stem cells, whereas Mll1 is redundant. Development. 2014;141(3):526-37.
758 Epub 2014/01/16. doi: 10.1242/dev.102681. PubMed PMID: 24423662.
759 41. el Marjou F, Janssen KP, Chang BH, Li M, Hindie V, Chan L, et al.
760 Tissue-specific and inducible Cre-mediated recombination in the gut
761 epithelium. Genesis. 2004;39(3):186-93. Epub 2004/07/30. doi:
762 10.1002/gene.20042. PubMed PMID: 15282745.
763 42. Yan KS, Gevaert O, Zheng GXY, Anchang B, Probert CS, Larkin KA, et
764 al. Intestinal Enteroendocrine Lineage Cells Possess Homeostatic and Injury-
765 Inducible Stem Cell Activity. Cell Stem Cell. 2017;21(1):78-90 e6. Epub
766 2017/07/08. doi: 10.1016/j.stem.2017.06.014. PubMed PMID: 28686870;
767 PubMed Central PMCID: PMCPMC5642297.
768 43. Munoz J, Stange DE, Schepers AG, van de Wetering M, Koo BK,
769 Itzkovitz S, et al. The Lgr5 intestinal stem cell signature: robust expression of
770 proposed quiescent '+4' cell markers. EMBO J. 2012;31(14):3079-91. Epub
771 2012/06/14. doi: 10.1038/emboj.2012.166. PubMed PMID: 22692129;
772 PubMed Central PMCID: PMCPMC3400017.
773 44. Haber AL, Biton M, Rogel N, Herbst RH, Shekhar K, Smillie C, et al. A
774 single-cell survey of the small intestinal epithelium. Nature.
775 2017;551(7680):333-9. Epub 2017/11/17. doi: 10.1038/nature24489. PubMed
776 PMID: 29144463; PubMed Central PMCID: PMCPMC6022292.
777 45. Zen K, Liu Y, McCall IC, Wu T, Lee W, Babbin BA, et al. Neutrophil
778 migration across tight junctions is mediated by adhesive interactions between
779 epithelial coxsackie and adenovirus receptor and a junctional adhesion
780 molecule-like protein on neutrophils. Mol Biol Cell. 2005;16(6):2694-703.
781 Epub 2005/04/01. doi: 10.1091/mbc.e05-01-0036. PubMed PMID: 15800062;
782 PubMed Central PMCID: PMCPMC1142417.
783 46. Kawabata K, Tashiro K, Sakurai F, Osada N, Kusuda J, Hayakawa T,
784 et al. Positive and negative regulation of adenovirus infection by CAR-like
785 soluble protein, CLSP. Gene Ther. 2007;14(16):1199-207. Epub 2007/06/01.
786 doi: 10.1038/sj.gt.3302975. PubMed PMID: 17538635.
787 47. Rodríguez-Colman MJ, Schewe M, Meerlo M, Stigter E, Gerrits J,
788 Pras-Raves M, et al. Interplay between metabolic identities in the intestinal
789 crypt supports stem cell function. Nature. 2017;543(7645):424-7. Epub
790 2017/03/09. doi: 10.1038/nature21673. PubMed PMID: 28273069.
791 48. Glaser S, Lubitz S, Loveland KL, Ohbo K, Robb L, Schwenk F, et al.
792 The histone 3 lysine 4 methyltransferase, Mll2, is only required briefly in
793 development and spermatogenesis. Epigenetics Chromatin. 2009;2(1):5. doi:

10.1186/1756-8935-2-5. PubMed PMID: 19348672; PubMed Central PMCID: PMC2674429.
49. Austenaa L, Barozzi I, Chronowska A, Termanini A, Ostuni R, Prosperini E, et al. The histone methyltransferase Wbp7 controls macrophage function through GPI glycolipid anchor synthesis. Immunity. 2012;36(4):572-85. doi: 10.1016/j.immuni.2012.02.016. PubMed PMID: 22483804.
50. Andreu-Vieyra CV, Chen R, Agno JE, Glaser S, Anastassiadis K, Stewart AF, et al. MLL2 is required in oocytes for bulk histone 3 lysine 4 trimethylation and transcriptional silencing. PLoS Biol. 2010;8(8). doi: 10.1371/journal.pbio.1000453. PubMed PMID: 20808952; PubMed Central PMCID: PMC2923083.
51. Hanna CW, Taudt A, Huang J, Gahurova L, Kranz A, Andrews S, et al. MLL2 conveys transcription-independent H3K4 trimethylation in oocytes. Nat Struct Mol Biol. 2018;25(1):73-82. Epub 2018/01/13. doi: 10.1038/s41594-017-0013-5. PubMed PMID: 29323282.
52. Artinger EL, Mishra BP, Zaffuto KM, Li BE, Chung EK, Moore AW, et al. An MLL-dependent network sustains hematopoiesis. Proc Natl Acad Sci U S A. 2013;110(29):12000-5. doi: 10.1073/pnas.1301278110. PubMed PMID: 23744037; PubMed Central PMCID: PMC3718146.
53. Carlone DL, Hart SR, Ladd PD, Skalnik DG. Cloning and characterization of the gene encoding the mouse homologue of CpG binding protein. Gene. 2002;295(1):71-7. Epub 2002/09/21. doi: 10.1016/s0378-1119(02)00820-x. PubMed PMID: 12242013.
54. Chang PY, Hom RA, Musselman CA, Zhu L, Kuo A, Gozani O, et al. Binding of the MLL PHD3 finger to histone H3K4me3 is required for MLL-dependent gene transcription. J Mol Biol. 2010;400(2):137-44. doi: 10.1016/j.jmb.2010.05.005. PubMed PMID: 20452361; PubMed Central PMCID: PMC2886590.
55. Guenther MG, Jenner RG, Chevalier B, Nakamura T, Croce CM, Canaani E, et al. Global and Hox-specific roles for the MLL1 methyltransferase. Proc Natl Acad Sci U S A. 2005;102(24):8603-8. doi: 10.1073/pnas.0503072102. PubMed PMID: 15941828; PubMed Central PMCID: PMC1150839.
56. Ernst P, Mabon M, Davidson AJ, Zon LI, Korsmeyer SJ. An Mll-dependent Hox program drives hematopoietic progenitor expansion. Curr Biol. 2004;14(22):2063-9. doi: 10.1016/j.cub.2004.11.012. PubMed PMID: 15556871.
57. Degar BA, Baskaran N, Hulspas R, Quesenberry PJ, Weissman SM, Forget BG. The homeodomain gene Pitx2 is expressed in primitive hematopoietic stem/progenitor cells but not in their differentiated progeny. Exp Hematol. 2001;29(7):894-902. Epub 2001/07/05. doi: 10.1016/s0301-472x(01)00661-0. PubMed PMID: 11438212.
58. Welsh IC, Thomsen M, Gludish DW, Alfonso-Parra C, Bai Y, Martin JF, et al. Integration of left-right Pitx2 transcription and Wnt signaling drives asymmetric gut morphogenesis via Daam2. Dev Cell. 2013;26(6):629-44. Epub 2013/10/05. doi: 10.1016/j.devcel.2013.07.019. PubMed PMID: 24091014; PubMed Central PMCID: PMCPMC3965270.
59. Ye DZ, Kaestner KH. Foxa1 and Foxa2 control the differentiation of goblet and enteroendocrine L- and D-cells in mice. Gastroenterology.

843 2009;137(6):2052-62. Epub 2009/09/10. doi: 10.1053/j.gastro.2009.08.059.
844 PubMed PMID: 19737569; PubMed Central PMCID: PMCPMC2789913.
845 60. van der Sluis M, Vincent A, Bouma J, Korteland-Van Male A, van
846 Goudoever JB, Renes IB, et al. Forkhead box transcription factors Foxa1 and
847 Foxa2 are important regulators of Muc2 mucin expression in intestinal
848 epithelial cells. Biochem Biophys Res Commun. 2008;369(4):1108-13. Epub
849 2008/03/14. doi: 10.1016/j.bbrc.2008.02.158. PubMed PMID: 18336786.
850 61. Wang P, Lin C, Smith ER, Guo H, Sanderson BW, Wu M, et al. Global
851 analysis of H3K4 methylation defines MLL family member targets and points
852 to a role for MLL1-mediated H3K4 methylation in the regulation of
853 transcriptional initiation by RNA polymerase II. Mol Cell Biol.
854 2009;29(22):6074-85. doi: 10.1128/MCB.00924-09. PubMed PMID:
855 19703992; PubMed Central PMCID: PMC2772563.
856 62. Beuling E, Baffour-Awuah NY, Stapleton KA, Aronson BE, Noah TK,
857 Shroyer NF, et al. GATA factors regulate proliferation, differentiation, and
858 gene expression in small intestine of mature mice. Gastroenterology.
859 2011;140(4):1219-29 e1-2. doi: 10.1053/j.gastro.2011.01.033. PubMed PMID:
860 21262227; PubMed Central PMCID: PMC3541694.
861 63. Tetteh PW. Plasticity of intestinal epithelial cells in regeneration and
862 cancer. Utrecht University; 2015.
863 64. Ritsma L, Ellenbroek SIJ, Zomer A, Snippert HJ, de Sauvage FJ,
864 Simons BD, et al. Intestinal crypt homeostasis revealed at single-stem-cell
865 level by in vivo live imaging. Nature. 2014;507(7492):362-5. Epub 2014/02/18.
866 doi: 10.1038/nature12972. PubMed PMID: 24531760; PubMed Central
867 PMCID: PMCPMC3964820.
868 65. Klymenko T, Muller J. The histone methyltransferases Trithorax and
869 Ash1 prevent transcriptional silencing by Polycomb group proteins. EMBO
870 Rep. 2004;5(4):373-7. doi: 10.1038/sj.embor.7400111. PubMed PMID:
871 15031712; PubMed Central PMCID: PMC1299022.
872 66. Douillet D, Sze CC, Ryan C, Piunti A, Shah AP, Ugarenko M, et al.
873 Uncoupling histone H3K4 trimethylation from developmental gene expression
874 via an equilibrium of COMPASS, Polycomb and DNA methylation. Nat Genet.
875 2020;52(6):615-25. Epub 2020/05/13. doi: 10.1038/s41588-020-0618-1.
876 PubMed PMID: 32393859.
877 67. Bledau AS, Schmidt K, Neumann K, Hill U, Ciotta G, Gupta A, et al.
878 The H3K4 methyltransferase Setd1a is first required at the epiblast stage,
879 whereas Setd1b becomes essential after gastrulation. Development.
880 2014;141(5):1022-35. doi: 10.1242/dev.098152. PubMed PMID: 24550110.
881 68. Anastassiadis K, Glaser S, Kranz A, Berhardt K, Stewart AF. A
882 practical summary of site-specific recombination, conditional mutagenesis,
883 and tamoxifen induction of CreERT2. Methods Enzymol. 2010;477:109-23.
884 Epub 2010/08/12. doi: 10.1016/s0076-6879(10)77007-5. PubMed PMID:
885 20699139.
886 69. Gregorieff A, Clevers H. In Situ Hybridization to Identify Gut Stem
887 Cells. Curr Protoc Stem Cell Biol. 2015;34:2F 1 -2F 1 11. doi:
888 10.1002/9780470151808.sc02f01s34. PubMed PMID: 26237569.
889 70. Nefzger CM, Jarde T, Rossello FJ, Horvay K, Knaupp AS, Powell DR,
890 et al. A Versatile Strategy for Isolating a Highly Enriched Population of
891 Intestinal Stem Cells. Stem Cell Reports. 2016;6(3):321-9. Epub 2016/03/01.

892 doi: 10.1016/j.stemcr.2016.01.014. PubMed PMID: 26923822; PubMed
893 Central PMCID: PMCPMC4788784.
894 71. Huang da W, Sherman BT, Lempicki RA. Systematic and integrative
895 analysis of large gene lists using DAVID bioinformatics resources. Nat Protoc.
896 2009;4(1):44-57. doi: 10.1038/nprot.2008.211. PubMed PMID: 19131956.
897 72. Subramanian A, Tamayo P, Mootha VK, Mukherjee S, Ebert BL,
898 Gillette MA, et al. Gene set enrichment analysis: a knowledge-based
899 approach for interpreting genome-wide expression profiles. Proc Natl Acad
900 Sci U S A. 2005;102(43):15545-50. Epub 2005/10/04. doi:
901 10.1073/pnas.0506580102. PubMed PMID: 16199517; PubMed Central
902 PMCID: PMCPMC1239896.
903 73. Livak KJ, Schmittgen TD. Analysis of relative gene expression data
904 using real-time quantitative PCR and the 2(-Delta Delta C(T)) Method.
905 Methods. 2001;25(4):402-8. doi: 10.1006/meth.2001.1262. PubMed PMID:
906 11846609.
907

908

909 ## Figure captions

910

911 **Fig 1. Loss of MLL1 in adult mice.** (A) Giemsa-stained sections from the
912 femur of *Mll1*$^{FC/+;\ RC/+}$ and *Mll1*$^{FC/FC;\ RC/+}$ mice. Two weeks after the last
913 tamoxifen gavage mice were sacrificed and the femurs were dissected,
914 decalcified, sectioned and stained. Bone marrow cellularity was severely
915 decreased in *Mll1*$^{FC/FC;\ RC/+}$ mice. Scale bar 100 µm. (B) Kaplan-Meier survival
916 curve. The first day of tamoxifen gavage was day zero. All *Mll1*$^{FC/+;\ RC/+}$ mice
917 (n=25) survived whereas all *Mll1*$^{FC/FC;\ RC/+}$ mice (n=33) died within 33 days
918 after tamoxifen induction with a median survival of 11 days. (C) Scheme of the
919 experimental setup for bone marrow transplantation. Donor bone marrow from
920 B6.SJL (CD45.1^{+}) mice was transplanted into lethally irradiated *Mll1*$^{F/+;\ RC/+}$
921 and *Mll1*$^{F/F;\ RC/+}$ recipients (CD45.2^{+}). Blood chimerism (BC) was measured
922 three times. After 30 weeks *Mll1* deletion was achieved by administrating
923 tamoxifen (TAM). FACS analysis for KSL-Slam enriched HSCs (Kit^{+} Sca1^{+}
924 Lin^{-} CD48^{-} CD150^{+} CD34^{-} CD135^{-}) showed comparable numbers in BMTx
925 *Mll1*$^{FC/+;\ RC/+}$ and *Mll1*$^{FC/FC;\ RC/+}$ mice. Dot plots show Lin^{-} CD48^{-} CD150^{+} CD34^{-}
926 CD135^{-} gated bone marrow (BM) cells of indicated genotypes resolved for the
927 expression of c-Kit and Sca-1. Donor and host cells are distinguished by
928 surface markers CD45.1 and CD45.2. (D) Kaplan-Meier analysis for the onset
929 of diarrhea. Tamoxifen was given by gavage for 6 days to *Mll1*$^{F/+;\ RC/+}$ (n=6)
930 and *Mll1*$^{F/F;\ RC/+}$ (n=8). The first day of tamoxifen gavage was day zero. While
931 all BMTx mice with the genotype *Mll1*$^{FC/+;\ RC/+}$ remained healthy, all BMTx
932 *Mll1*$^{FC/FC;\ RC/+}$ mice developed diarrhea with a median of 16.5 days. (E)
933 Antibody staining (brown) showed that MLL1 is expressed in crypts of the

934 small and large intestine but absent in the villus (hematoxylin, purple). Scale
935 bars are 50 μm.
936
937 **Fig 2. *Mll1* deletion in BMTx mice leads to loss of stem and proliferating**
938 **cells and increased goblet cells.** (A) Antibody stainings showed reduced
939 MLL1, OLFM4 and SOX9 expression in BMTx *Mll1*$^{FC/FC;\ RC/+}$ intestine
940 compared to controls. Hematoxylin was used as a counterstain for MLL1 and
941 OLFM4 immunohistochemistry (IHC). Expression of Ki67, a marker for
942 proliferating cells was reduced in BMTx *Mll1*$^{FC/FC;\ RC/+}$ mutant intestinal
943 sections. Arrowheads point toward proliferating ISCs. Alcian blue was used as
944 a counterstain for SOX9 and Ki67 IHC, which also revealed enlarged goblet
945 cells (turquoise) in the crypts of BMTx *Mll1*$^{FC/FC;\ RC/+}$ sections. Scale bars are
946 50 μm. (B) PAS stain to examine goblet cells in villi and crypts of BMTx
947 intestine. Black arrowheads point towards vacuolar structures. Yellow
948 arrowhead points to a mislocalized goblet cell in BMTx *Mll1*$^{FC/FC;\ RC/+}$ crypt.
949 Left panels scale bar 100 μm; middle panels scale bar 50 μm. GOB5 antibody
950 staining of BMTx *Mll1*$^{FC/FC;\ RC/+}$ intestinal sections. Right panels scale bar 100
951 μm. (C) Left panels; lysozyme antibody staining reveals that Paneth cell
952 numbers remain unchanged. Arrowheads point at Paneth cells. Alcian blue
953 was used as a counterstain and marks goblet cells (turquoise). Middle panels;
954 chromogranin A antibody stain, arrowheads point to the sparse
955 enteroendocrine cells (dark brown) in the villi. Right panels; red enterocytes
956 covering the villi were visualized by alkaline phosphatase staining.
957 Hematoxylin was used as a counterstain for chromogranin A IHC and alkaline
958 phosphatase histochemical staining. Scale bars are 50 μm.

959 **Fig 3. Decreased ISCs and increased goblet cells after intestinal specific**
960 **loss of MLL1.** (A) Percent of weight loss of *Mll1*$^{FC/+;\ Vil\text{-}Cre\text{-}ERT2/+}$ (n=5) and of
961 *Mll1*$^{FC/FC;\ Vil\text{-}Cre\text{-}ERT2/+}$ (n=9) mice. Mean ± s.d. is shown (p=0.029, Student's *t*-
962 test). (B) Decrease in ISC markers, OLFM4 and SOX9 in *Mll1*$^{FC/FC;\ Vil\text{-}Cre\text{-}ERT2/+}$
963 intestinal sections. SOX9^{+} ISCs in *Mll1*$^{FC/+;\ Vil\text{-}Cre\text{-}ERT2/+}$ intestinal sections are
964 marked with red arrowheads. Proliferating cells in the TA compartment as well
965 as proliferative ISCs (arrowhead) are reduced in *Mll1*$^{FC/FC;\ Vil\text{-}Cre\text{-}ERT2/+}$ sections.
966 Alcian blue was used as a counterstain after staining for SOX9 and Ki67 and
967 marks goblet cells (turquoise). Scale bars are 100 μm for OLFM4 and 50 μm
968 for SOX9 and Ki67. (C) Left panels; alcian blue staining of goblet cells with
969 nuclear fast red (NFR) to stain nuclei. Middle panels; Paneth cells visualized
970 by staining of granules containing lysozyme (arrowheads). Right panels;
971 enteroendocrine cells stained with chromogranin A antibody (brown;
972 arrowheads) in the villi. Scale bars are 100 μm.
973
974 **Fig 4. RNA profiling of *Mll1*$^{FC/FC;\ Lgr5\text{-}eGFP\text{-}CreERT2/+}$ and control ISCs.** (A)
975 ISCs were sorted from control (*Mll1*$^{FC/+;\ Lgr5\text{-}eGFP\text{-}CreERT2/+}$) (n=4) and *Mll1*$^{FC/FC;}$
976 $^{Lgr5\text{-}eGFP\text{-}CreERT2/+}$ (n=4) mice 4 days after tamoxifen induction was completed
977 and subjected to RNA profiling. MA plot visualizing the log2-fold change
978 differences according to expression levels of ISCs. Red dots represent
979 significant DEGs at a 5% FDR. *Jaml* is the top downregulated gene. (B) Plots
980 show biological processes (BP) that are enriched in genes up- or
981 downregulated in *Mll1*$^{FC/FC;\ Lgr5\text{-}eGFP\text{-}CreERT2/+}$ compared to control ISCs.
982 Analysis was performed using the gene ontology (GO)/BP/FAT database of
983 DAVID 6.8. (C) (D) GSEA shows significant negative or positive correlation of

984 genes from the stem (C) and goblet cell (D) signature gene set in *Mll1*$^{FC/FC;}$
985 $^{Lgr5\text{-}eGFP\text{-}CreERT2/+}$ compared to control ISCs (4 days after tamoxifen). The
986 signature gene sets originate from [44]. NES: normalized enrichment score.
987 (E) DESeq normalized counts for genes coding for transcription factors
988 downregulated in *Mll1*$^{FC/FC;\ Lgr5\text{-}eGFP\text{-}CreERT2/+}$ compared to control ISCs (4 days
989 after tamoxifen). Mean+s.d. is shown; n=4; p<0.05, Wald test. (F) DESeq
990 normalized counts for genes coding for ISC markers downregulated in
991 *Mll1*$^{FC/FC;\ Lgr5\text{-}eGFP\text{-}CreERT2/+}$ compared to control ISCs (4 days after tamoxifen).
992 Mean+s.d. is shown; n=4; p<0.05, Wald test (G) DESeq normalized counts for
993 genes coding for goblet cell markers upregulated in *Mll1*$^{FC/FC;\ Lgr5\text{-}eGFP\text{-}CreERT2/+}$
994 compared to control ISCs (4 days after tamoxifen). Mean+s.d. is shown; n=4;
995 p<0.05, Wald test.
996
997 **Fig 5. RNA profiling of wt Paneth cells after deletion of *Mll1* in the**
998 **neighboring ISCs.** (A) Wt Paneth cells neighboring either *Mll1*$^{FC/+;\ Lgr5\text{-}eGFP\text{-}}$
999 $^{CreERT2/+}$ or *Mll1*$^{FC/FC;\ Lgr5\text{-}eGFP\text{-}CreERT2/+}$ ISCs were sorted 4 days after tamoxifen
1000 induction was completed and were subjected to RNA profiling. MA plot
1001 visualizing the log2-fold change differences according to expression levels of
1002 Paneth cells. Red dots represent significant DEGs at a 5% FDR. (B) Enriched
1003 terms of biological processes and pathways down- and upregulated using
1004 DAVID GO/BP/FAT and KEGG database. (C) GSEA shows significant
1005 negative or positive correlation of genes from the GO ERAD pathway, GO
1006 oxidative phosphorylation and Paneth cell signature gene set in wt Paneth
1007 cells neighboring either *Mll1*$^{FC/FC;\ Lgr5\text{-}eGFP\text{-}CreERT2/+}$ or *Mll1*$^{FC/+;\ Lgr5\text{-}eGFP\text{-}CreERT2/+}$
1008 ISCs. The Paneth cell signature gene set originates from [44]. NES:

1009 normalized enrichment score. (D) DESeq normalized counts for selected
1010 genes differentially regulated in the ERAD pathway, oxidative phosphorylation
1011 and Paneth cell signature gene set. Mean+s.d. is shown; n=4; $p<0.05$, Wald
1012 test.
1013
1014 **Fig 6. *Mll1* deletion in organoids results in formation of spheres.** (A)
1015 Differential interference contrast (DIC) images of *Mll1*$^{FC/+;\ RC/+}$ and *Mll1*$^{FC/FC;}$
1016 $^{RC/+}$ organoids. Organoids were induced with 4-OH tamoxifen for 24 h. Upon
1017 passaging (P), the mutant starts to loose its budding morphology giving rise to
1018 an undifferentiated cyst-like appearance. Scale bar 100 µm. (B) Genotyping of
1019 organoids/spheres for *Mll1* at passage 2. After tamoxifen induction the *Mll1*^{F}
1020 allele recombines and results in the *Mll1*^{FC} allele. PCR primers located
1021 upstream of the 5' FRT site and downstream of the 3' loxP site (see S1A Fig)
1022 identify the respective band. Consequently, the *Mll1*^{F} band is 1084 bp, the wt
1023 band is 933 bp and the *Mll1*^{FC} band is 186 bp. An additional PCR was
1024 performed with primers flanking the 3' loxP site. Consequently, the *Mll1*^{F} band
1025 is 297 bp and the wt band is 251 bp. (C) Quantification of organoids and
1026 spheres shown in A. (D) qRT-PCR was performed for selected genes on
1027 cDNA from *Mll1*$^{FC/+;\ RC/+}$ and *Mll1*$^{FC/FC;\ RC/+}$ organoid culture. Mean+s.d. is
1028 shown; n=3; *$p<0.05$, **$p<0.01$, ***$p<0.001$, Student's *t* test.
1029
1030 **Fig 7. Cell-cell contacts are essential for cell identity.** JAML is an integral
1031 transmembrane protein expressed on ISCs and interacts with unknown
1032 proteins on Paneth cells. Loss of MLL1 in ISCs causes loss of JAML mediated

1033 interactions, transcriptional changes and subsequently loss of stem and
1034 Paneth cell identity.

1035 ## Supporting information

1036

1037 **S1 Fig. *Mll1* gene targeting, embryonic phenotype and aspects of**
1038 **expression. (A)** Diagram of the *Mll1* gene with numbered exons and the
1039 multipurpose allele ($Mll1^{A}$). This allele is converted to $Mll1^{F}$ upon FLP
1040 recombination. Cre recombination leads to excision of the frameshifting exon
1041 2 generating the conditional mutant allele ($Mll1^{FC}$). Genotyping primers are
1042 depicted for the downstream loxP site (loxP1 – loxP2) and for Flp
1043 recombination (Flp se – loxP2). SA = splice acceptor, IRES = internal
1044 ribosome entry site, pA = polyadenylation signal, lacZ-neo = β-galactosidase
1045 and neomycin resistance gene, * depicts premature stop codon. **(B)**
1046 Schematic representation of the Southern blot strategy. For identifying correct
1047 targeted events in the *Mll1* locus, Southern blot analysis employed 5' (blue
1048 box) and 3' (red box) probes. **(C)** Southern blot analysis using 5' and 3'
1049 external probes. **(D)** Dissected embryos from $Mll1^{A/+}$ intercrosses at E12.5.
1050 $Mll1^{A/A}$ embryos had a pale liver (marked by arrow). **(E)** Antibody staining
1051 (brown) shows that MLL1 is expressed in crypts and TA compartment of the
1052 small intestine but is absent in the villus (hematoxylin, purple). Scale bar 50
1053 µm. **(F)** Normalized RNA-sequence counts for *Mll1/Kmt2a, Mll2/Kmt2b,*
1054 *Mll3/Kmt2c, Mll4/Kmt2d, Setd1a/Kmt2f and Setd1b/Kmt2g* in ISCs ($eGFP^{high}$)
1055 and Paneth cells sorted from *Lgr5-eGFP-CreERT2* mice. Mean+s.d. is shown;
1056 n=4; *p<0.05, **p<0.01, ***p<0.001, ****p<0.0001, Student's *t* test. **(G)**
1057 Antibody stainings of H3K4me1, H3K4me2 and H3K4me3 are comparable in
1058 $Mll1^{FC/+;\ RC/+}$ and $Mll1^{FC/FC;\ RC/+}$ intestinal sections. Scale bars are 100 µm.

1059

1060 **S2 Fig. Without bone marrow transplantation, *Mll1* deletion recapitulates**
1061 **the BMTx *Mll1* mutant phenotype. (A)** Antibody stain (left panels) and *in situ*
1062 hybridization (right panels) to visualize OLFM4/*Olfm4* in intestinal sections.
1063 Arrowheads point towards ISCs. Scale bar 100 μm. **(B)** Proliferative activity
1064 visualized by both Ki67 stain and BrdU incorporation in intestinal sections.
1065 Arrowheads point towards proliferative ISCs. Scale bars are 50 μm. **(C)** PAS
1066 staining and GOB5 antibody stain to visualize goblet cells in intestinal
1067 sections. Scale bars are 100 μm. **(D)** Chromogranin A and alkaline
1068 phosphatase staining to visualize enteroendocrine cells and enterocytes
1069 respectively. Arrows point to enteroendocrine cells (brown cytoplasmic stain)
1070 in the villi. Blue enterocytes covering the villi are marked by arrowheads.
1071 Scale bars are 100 μm for chromogranin A and 50 μm for alkaline
1072 phosphatase. **(E)** Nuclear β-catenin is comparable between the two different
1073 genotypes. Arrowheads point at β-catenin positive nuclei. Scale bar is 50 μm.
1074

1075 **S3 Fig. FACS gating strategy to sort ISCs and Paneth cells.** Flow sorting
1076 on **(A)** *Mll1*$^{FC/+;\ Lgr5\text{-}eGFP\text{-}CreERT2/+}$ and **(B)** *Mll1*$^{FC/FC;\ Lgr5\text{-}eGFP\text{-}CreERT2/+}$ single cell
1077 suspension of crypts. Briefly, the consecutive gating steps were applied: (i) –
1078 (iii) Definition of the population of interest by exclusion of debris based on size
1079 (FSC), granularity (SSC) and the selection for single cells; (iv) Exclusion of
1080 dead cells that incorporated the nucleic acid stain SYTOX blue; (v) Depletion
1081 of CD45^{pos} population; (vi) Definition of Paneth (EpCAM^{high}/CD24^{high}) cell
1082 population by plotting EpCAM vs CD24 fluorescence; (vii) EpCAM^{high}/CD24^{med}
1083 cell population was gated to discriminate the stem cell population (GFP^{high}).
1084 **(C)** Stem cells (SC) and Paneth cells (PC) from *Mll1*$^{FC/+;\ Lgr5\text{-}eGFP\text{-}CreERT2/+}$ and

1085 *Mll1*$^{FC/FC;\ Lgr5\text{-}eGFP\text{-}CreERT2/+}$ mice 4 days after tamoxifen induction were checked
1086 for recombination. Left panel; PCR genotyping was using primers upstream of
1087 the 5' FRT site and downstream of the 3' loxP site identified the *Mll1*^{F} band at
1088 1084 bp, the wild type band a 933 bp and the *Mll1*^{FC} band at 186 bp. Right
1089 panel; primers flanking the 3' loxP site identified the *Mll1*^{F} band at 297 bp and
1090 the wild type band at 251 bp.
1091
1092 **S4 Fig. Alignment and quality of the sequenced data. (A)** ISCs and
1093 Paneth cells were analyzed from control (*Mll1*$^{FC/+;\ Lgr5\text{-}eGFP\text{-}CreERT2/+}$) (ctrl) (n=4)
1094 and *Mll1*$^{FC/FC;\ Lgr5\text{-}eGFP\text{-}CreERT2/+}$ (n=4) (KO) mice. Mappability of reads for sorted
1095 ISCs 4 days after tamoxifen induction was completed. **(B)** Mappability of
1096 reads for sorted Paneth cells 4 days after tamoxifen induction was completed.
1097 **(C)** Mappability of reads for sorted ISCs 10 days after tamoxifen induction was
1098 completed. ISCs were analyzed from control (*Mll1*$^{FC/+;\ Lgr5\text{-}eGFP\text{-}CreERT2/+}$) (ctrl)
1099 (n=4) and *Mll1*$^{FC/FC;\ Lgr5\text{-}eGFP\text{-}CreERT2/+}$ (n=3) (KO) mice. **(D)** Principal-component
1100 analysis (PCA) was performed on Paneth cell and ISC samples sorted 4 days
1101 after tamoxifen. PCA is based on mRNA changes for the top 500 most diverse
1102 genes of stem cell (SC) and Paneth cell (PC) samples in comparison to
1103 published datasets for Lgr5^{+} SC [42] and CD24^{+} PC [35].
1104
1105 **S5 Fig. ISCs lacking MLL1 loose their cellular identity. (A) (B)** GSEA
1106 shows significant negative or positive correlation of genes from the stem (A)
1107 and goblet cell (B) signature gene set in *Mll1*$^{FC/FC;\ Lgr5\text{-}eGFP\text{-}CreERT2/+}$ ISCs
1108 compared to control ISCs 10 days after tamoxifen induction was completed.
1109 The signature gene sets originate from [44]. NES: normalized enrichment

1110 score. **(C)** To validate RNA-seq results qRT-PCR was performed for selected
1111 genes on cDNA from *Mll1*$^{FC/+;\ Lgr5\text{-}eGFP\text{-}CreERT2/+}$ and *Mll1*$^{FC/FC;\ Lgr5\text{-}eGFP\text{-}CreERT2/+}$
1112 sorted stem cells 4 days after tamoxifen induction was completed. Mean+s.d.
1113 is shown; n=3; *p<0.05, **p<0.01, Student's *t* test. **(D)** DESeq normalized
1114 counts demonstrate *Jaml* being highly expressed in Lgr5^{+} ISCs but not in
1115 Paneth cells. Mean+s.d. is shown; n=4; ***p<0.001, Student's *t* test.
1116

Fig 1.

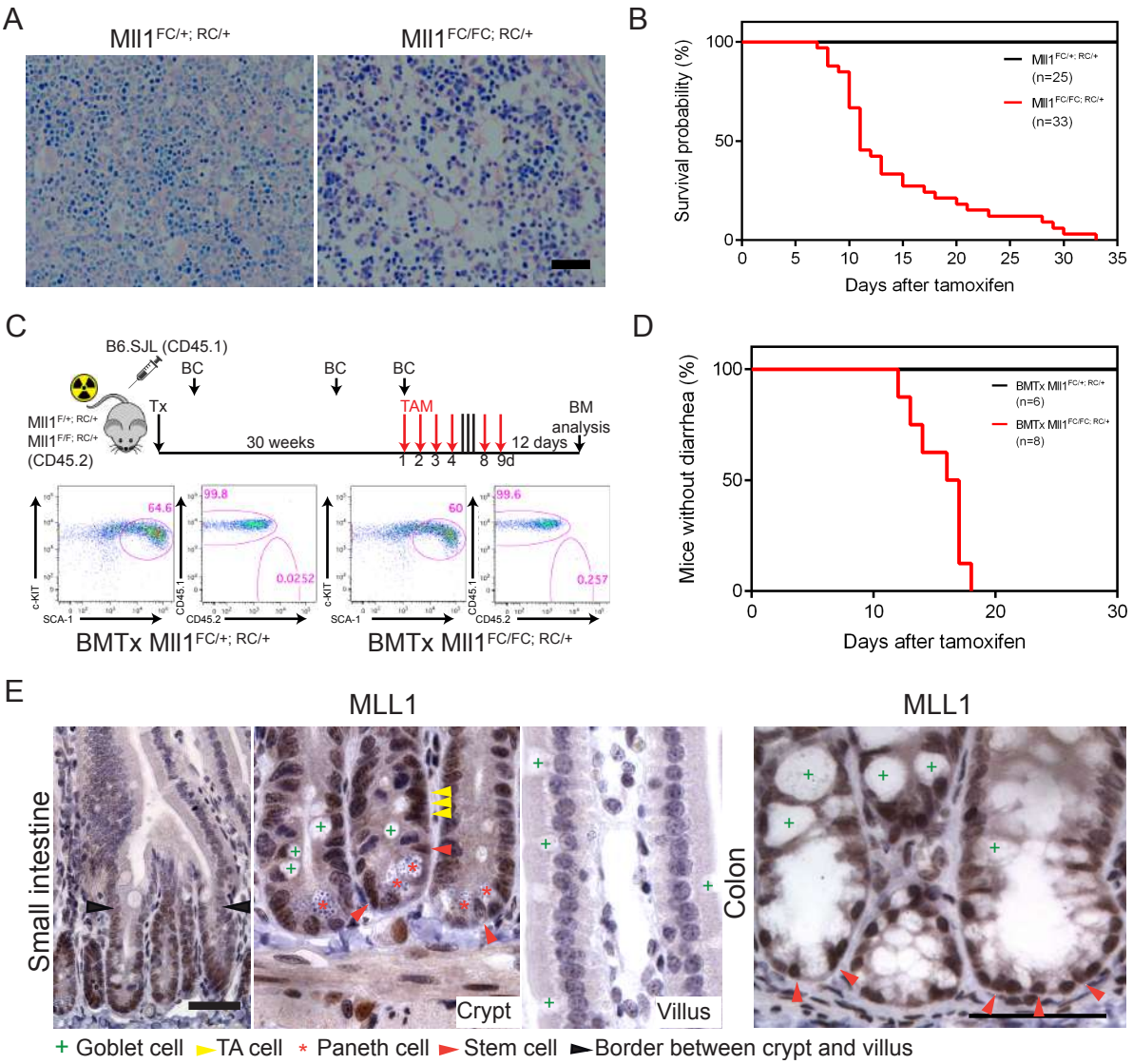
A
Mll1FC/+; RC/+
Mll1FC/FC; RC/+
B
Survival probability (%)
100
50
0
0 5 10 15 20 25 30 35
Days after tamoxifen
Mll1FC/+; RC/+ (n=25)
Mll1FC/FC; RC/+ (n=33)
C
B6.SJL (CD45.1)
BC
BC
BC
Tx
TAM
BM analysis
Mll1F/+; RC/+
Mll1F/F; RC/+
(CD45.2)
30 weeks
12 days
1 2 3 4 8 9d
64.6
99.8
0.0252
60
99.6
0.257
c-KIT
SCA-1
CD45.1
CD45.2
BMTx Mll1FC/+; RC/+
BMTx Mll1FC/FC; RC/+
D
Mice without diarrhea (%)
100
50
0
0 10 20 30
Days after tamoxifen
BMTx Mll1FC/+; RC/+ (n=6)
BMTx Mll1FC/FC; RC/+ (n=8)
E
MLL1
MLL1
Small intestine
Colon
Crypt
Villus
+ Goblet cell
TA cell
* Paneth cell
Stem cell
Border between crypt and villus

Fig 2.

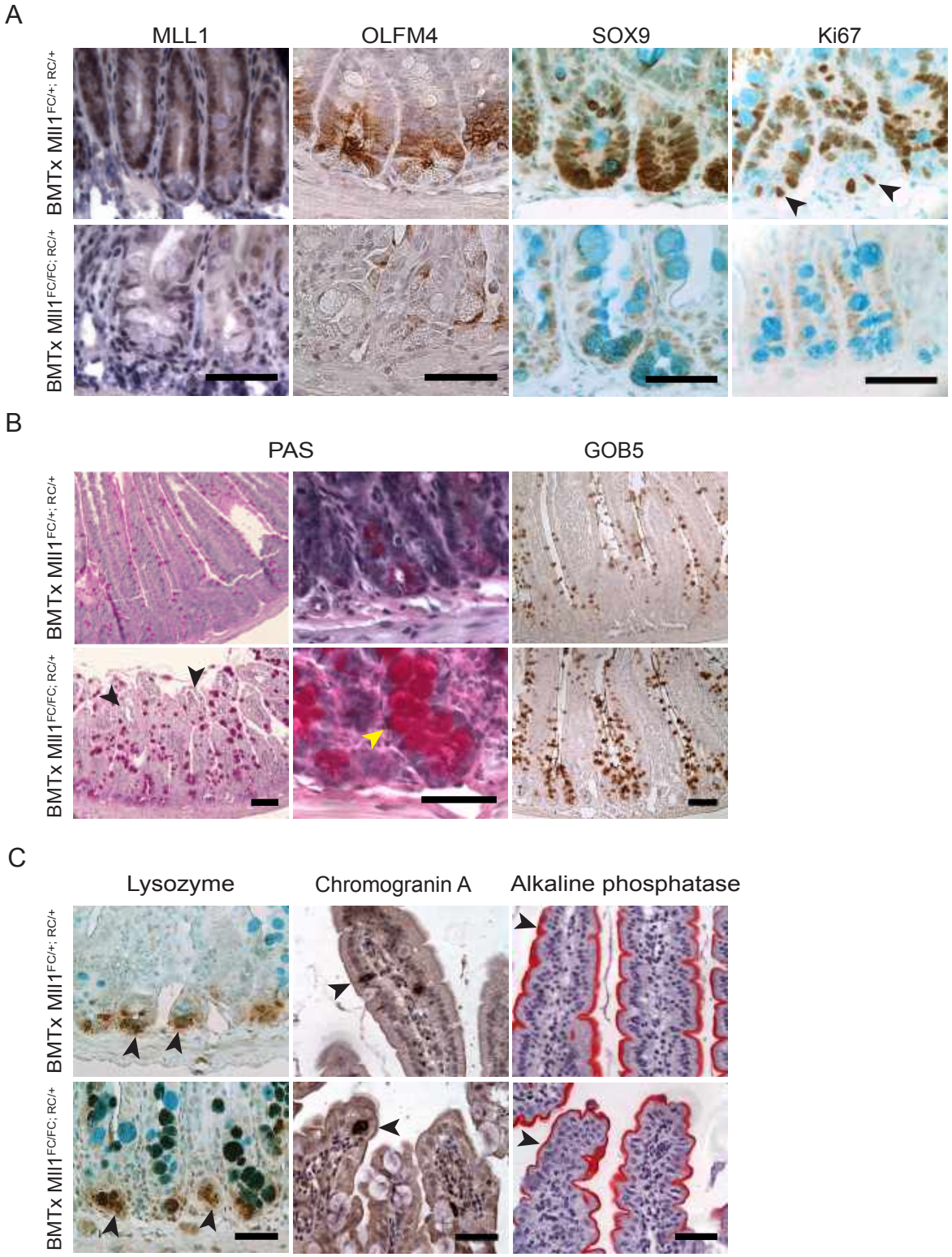
A
MLL1
OLFM4
SOX9
Ki67
BMTx Mll1FC/+; RC/+
BMTx Mll1FC/FC; RC/+
B
PAS
GOB5
BMTx Mll1FC/+; RC/+
BMTx Mll1FC/FC; RC/+
C
Lysozyme
Chromogranin A
Alkaline phosphatase
BMTx Mll1FC/+; RC/+
BMTx Mll1FC/FC; RC/+

Fig 3.

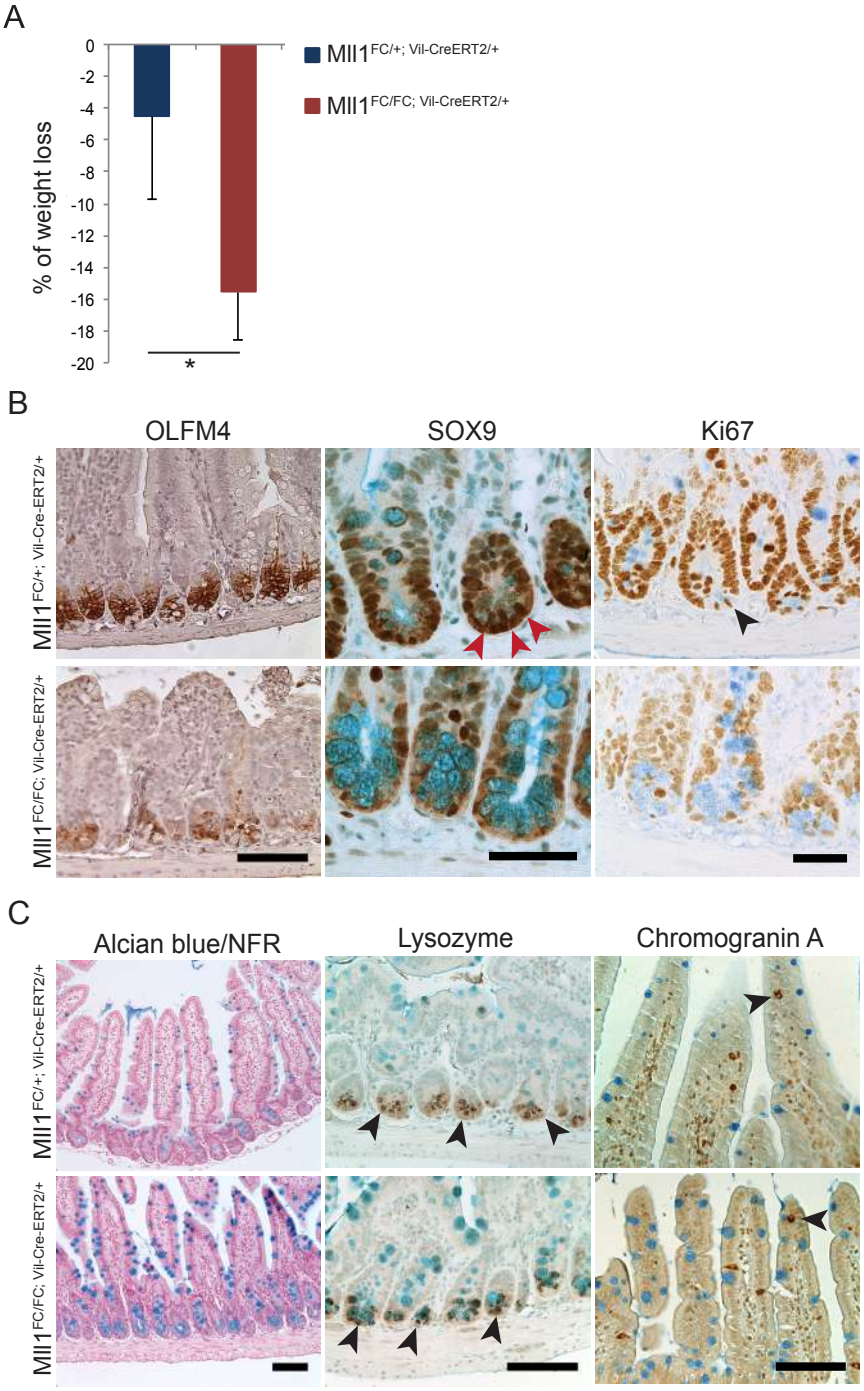
A
% of weight loss
0
-2
-4
-6
-8
-10
-12
-14
-16
-18
-20
*
Mll1 FC/+; Vil-CreERT2/+
Mll1 FC/FC; Vil-CreERT2/+
B
OLFM4
SOX9
Ki67
Mll1 FC/+; Vil-Cre-ERT2/+
Mll1 FC/FC; Vil-Cre-ERT2/+
C
Alcian blue/NFR
Lysozyme
Chromogranin A
Mll1 FC/+; Vil-Cre-ERT2/+
Mll1 FC/FC; Vil-Cre-ERT2/+

Fig 4.

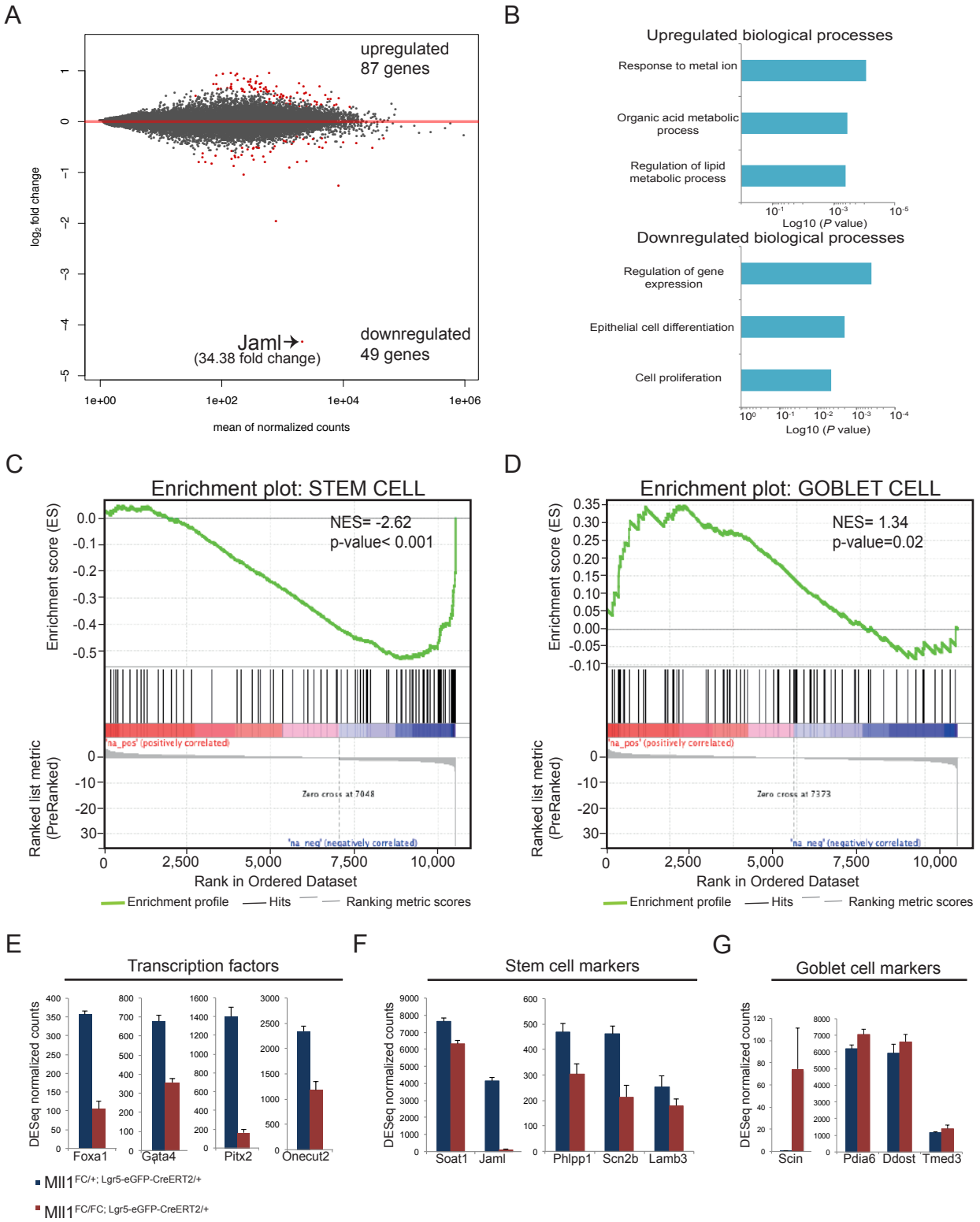
A
upregulated
87 genes
downregulated
49 genes
Jaml
(34.38 fold change)
log2 fold change
mean of normalized counts
B
Upregulated biological processes
Response to metal ion
Organic acid metabolic process
Regulation of lipid metabolic process
Log10 (P value)
Downregulated biological processes
Regulation of gene expression
Epithelial cell differentiation
Cell proliferation
Log10 (P value)
C
Enrichment plot: STEM CELL
NES= -2.62
p-value< 0.001
Enrichment score (ES)
Ranked list metric (PreRanked)
Rank in Ordered Dataset
Enrichment profile
Hits
Ranking metric scores
D
Enrichment plot: GOBLET CELL
NES= 1.34
p-value=0.02
Enrichment score (ES)
Ranked list metric (PreRanked)
Rank in Ordered Dataset
Enrichment profile
Hits
Ranking metric scores
E
Transcription factors
DESeq normalized counts
Foxa1
Gata4
Pitx2
Onecut2
F
Stem cell markers
DESeq normalized counts
Soat1
Jaml
Phlpp1
Scn2b
Lamb3
G
Goblet cell markers
DESeq normalized counts
Scin
Pdia6
Ddost
Tmed3
Mll1 FC/+; Lgr5-eGFP-CreERT2/+
Mll1 FC/FC; Lgr5-eGFP-CreERT2/+

Fig 5.

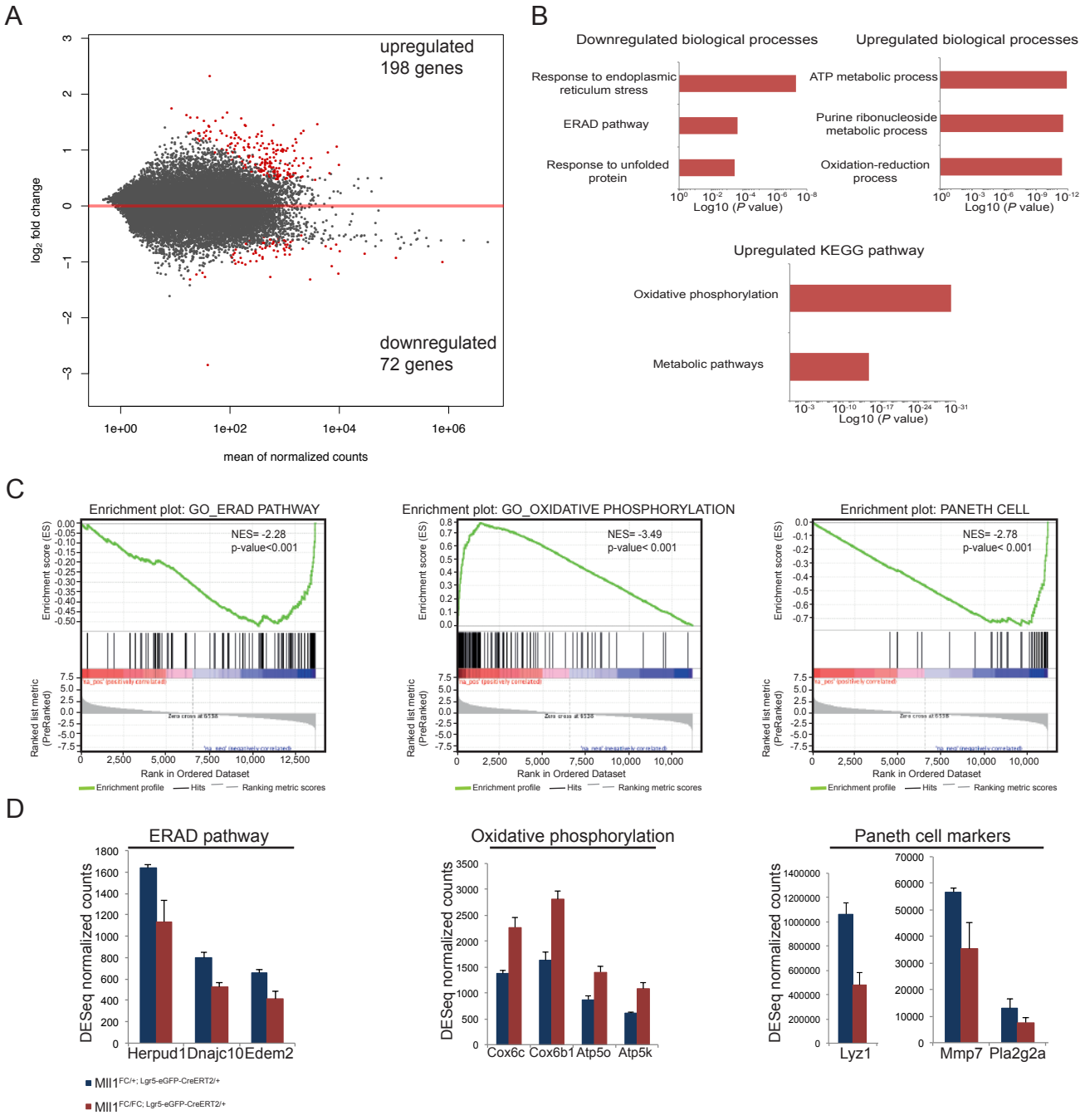
A
upregulated
198 genes
downregulated
72 genes
log2 fold change
mean of normalized counts
B
Downregulated biological processes
Response to endoplasmic reticulum stress
ERAD pathway
Response to unfolded protein
Log10 (P value)
Upregulated biological processes
ATP metabolic process
Purine ribonucleoside metabolic process
Oxidation-reduction process
Log10 (P value)
Upregulated KEGG pathway
Oxidative phosphorylation
Metabolic pathways
Log10 (P value)
C
Enrichment plot: GO_ERAD PATHWAY
NES= -2.28
p-value<0.001
Enrichment plot: GO_OXIDATIVE PHOSPHORYLATION
NES= -3.49
p-value< 0.001
Enrichment plot: PANETH CELL
NES= -2.78
p-value< 0.001
Enrichment score (ES)
Ranked list metric (PreRanked)
Rank in Ordered Dataset
Enrichment profile
Hits
Ranking metric scores
D
ERAD pathway
Herpud1
Dnajc10
Edem2
Oxidative phosphorylation
Cox6c
Cox6b1
Atp5o
Atp5k
Paneth cell markers
Lyz1
Mmp7
Pla2g2a
DESeq normalized counts
Mll1FC/+; Lgr5-eGFP-CreERT2/+
Mll1FC/FC; Lgr5-eGFP-CreERT2/+

Fig 6.

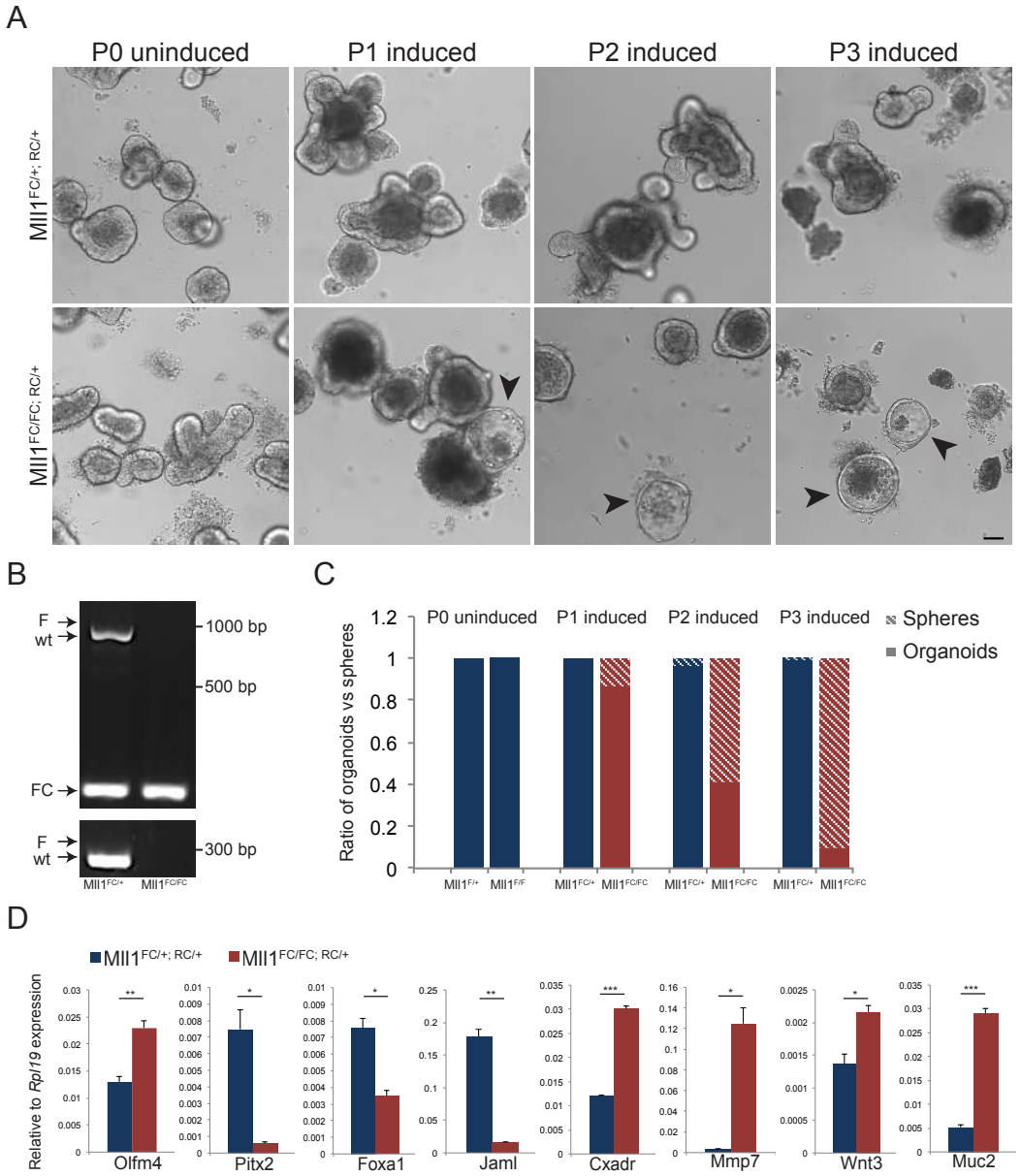
A
P0 uninduced
P1 induced
P2 induced
P3 induced
Mll1FC/+; RC/+
Mll1FC/FC; RC/+
B
F
wt
FC
1000 bp
500 bp
300 bp
Mll1FC/+
Mll1FC/FC
C
Ratio of organoids vs spheres
Spheres
Organoids
Mll1F/+
Mll1F/F
D
Relative to Rpl19 expression
Olfm4
Pitx2
Foxa1
Jaml
Cxadr
Mmp7
Wnt3
Muc2

Fig 7.

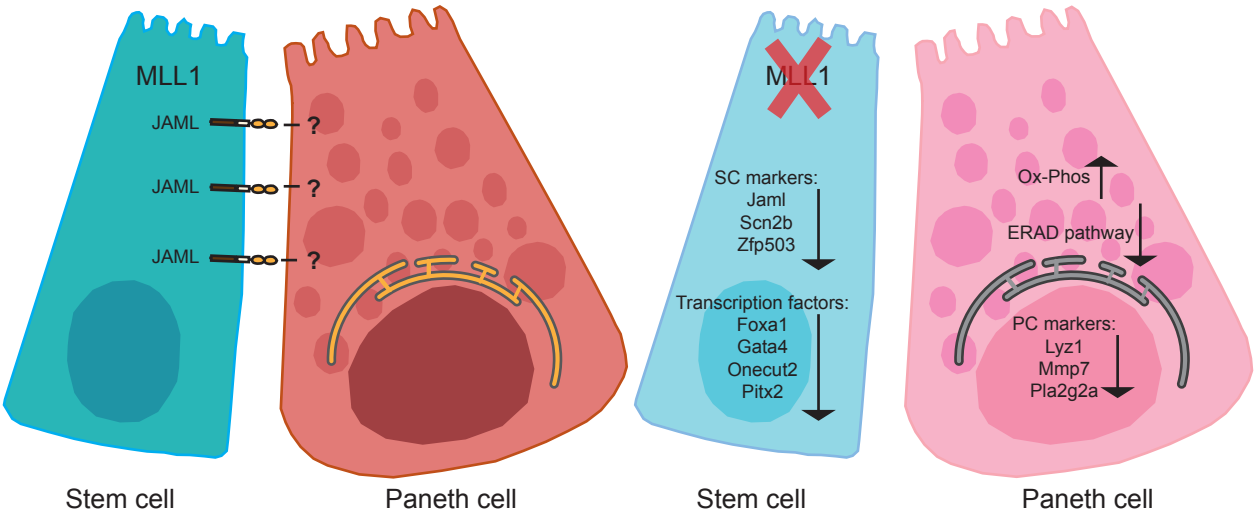
MLL1
JAML
?
JAML
?
JAML
?
Stem cell
Paneth cell
MLL1
SC markers:
Jaml
Scn2b
Zfp503
Transcription factors:
Foxa1
Gata4
Onecut2
Pitx2
Stem cell
Ox-Phos
ERAD pathway
PC markers:
Lyz1
Mmp7
Pla2g2a
Paneth cell